ORIGINAL PAPER

Interpretation of Core Extrusion Measurements When Tunnelling Through Squeezing Ground

L. Cantieni · G. Anagnostou · R. Hug

Abstract Squeezing intensity in tunnelling often varies over short distances, even where there is no change in the excavation method or lithology. Reliable predictions of the ground conditions ahead of the face are thus essential to avoid project setbacks. Such predictions would enable adjustments to be made during construction to the temporary support, to the excavation diameter and also to the final lining. The assessment of the behaviour of the core ahead of the face, as observed by means of extrusion measurements, provides some indications as to the mechanical characteristics of the ground. If the ground exhibits a moderate time-dependent behaviour and the effects of the support measures are taken into account, the prediction of convergence is feasible. If the ground behaviour is pronouncedly time-dependent, however, convergence predictions become very difficult, because core extrusion is governed by the short-term characteristics of the ground, which may be different from the long-term properties that govern final convergence. The case histories of the Gotthard Base Tunnel and of the Vasto tunnel show that there is a weak correlation between the axial extrusions and the convergences of the tunnel. By means of the case histories of the Tartaiguille tunnel and Raticosa tunnel, it is shown that to identify potentially weak zones on the basis of the extrusion measurements, careful processing of the monitoring data is essential: the analysis of the data has to take account of the effects of tunnel support and time, and has to eliminate errors caused by the monitoring process.

List of Symbols

a	Tunnel radius
A_F	Area of the tunnel face
b	Lining thickness
c'	Effective cohesion of the ground
d	Distance between tunnel face and measuring point on the tunnel axis
d_c	Distance between tunnel face and measuring point on the tunnel boundary
E	Young's modulus of the ground
E_L	Young's modulus of the lining
e	Unsupported span
$f_i()$	Function ($i = 1, 2, 3, \ldots$)
f	Yield function
f_c	Uniaxial compressive strength of the ground
g	Plastic potential
H	Overburden
k	Radial stiffness of a ring-shaped lining
$L_{i,t}$	Distance between the reference point R and point i ($i = $ A, B) at time t
$L_{i,0}$	Initial distance between the reference point R and point i ($i = $ A, B)
$p(y)$	Radial pressure at the tunnel boundary
p_0	Initial stress
p_y	Yield pressure of the tunnel support
r	Radial co-ordinate (distance from tunnel axis)
s	Round length in the step-by-step calculations
S	Face advance (multiple of s)

L. Cantieni (✉) · G. Anagnostou · R. Hug
ETH Zurich, Switzerland
e-mail: linard.cantieni@igt.baug.ethz.ch

Present Address:
R. Hug
Ernst Basler & Partner AG, Zurich, Switzerland

t	Time
u	Displacement of the ground
u_r	Radial displacement of the ground at the tunnel boundary
u_c	Radial ground displacement developing behind the face (convergence)
u_y	Axial displacement of the ground at the tunnel axis
$u_{y,i}$	Axial displacement of the point i at the tunnel axis (i = A, B, O, R)
v	Advance rate of the excavation
y	Axial co-ordinate
y_i	Axial co-ordinate of Point i (i = A, B)
y_F	Axial co-ordinate of the tunnel face

Greek Symbols

$\Delta u_{y,A}(d, S)$	Change in axial displacement of point A caused by a face advance of S (d denotes the distance of point A from the face after the face advance)
ε_y	Axial strain of the ground at the tunnel axis
$\varepsilon_{y,AB}(d)$	Average axial strain of the ground between the points A and B, whereby Point A is located at distance d ahead of the face
$\varepsilon_{t,c}$	Tangential ground strain at the tunnel boundary developing behind the face (convergence normalized by the tunnel radius)
$\Delta \varepsilon_{t,c}$	Change in tangential ground strain at the tunnel boundary for a specific face advance
$\Delta L_{A,t}$	Change in the distance of point A from reference point R at time t
$\Delta L_{B,t}$	Change in the distance of point B from reference point R at time t
$\dot{\varepsilon}_{ij}$	Strain rate tensor
$\dot{\varepsilon}_{ij}^e$	Elastic part of the strain rate tensor $\dot{\varepsilon}_{ij}$
$\dot{\varepsilon}_{ij}^p$	Inelastic part of the strain rate tensor $\dot{\varepsilon}_{ij}$
η	Viscosity
ν	Poisson's ratio of the ground
σ_r	Radial stress
φ	Angle of internal friction of the ground
φ'	Effective angle of internal friction of the ground
ψ	Dilatancy angle of the ground

1 Introduction

Squeezing intensity can vary greatly over short distances even where there is no change in the excavation method, temporary support, depth of cover or lithology (Kovári 1998). This variability makes tunnelling in squeezing ground very demanding, as it decreases the predictability of the conditions ahead of the face even after some experience

has been gained with a specific geological formation during excavation. The variability can be traced back to two different reasons (Cantieni and Anagnostou 2007): (1) rock structure heterogeneity (even on the scale of few meters) may lead to significant variations in the ground response; and, (2), small fluctuations in the mechanical and hydraulic properties of a macroscopically homogeneous rock mass may have a major effect on the development of deformations and pressures.

Uncertainties concerning rock structure heterogeneity can be reduced by advance probing. However, the uncertainties concerning ground response will remain. Therefore, the prediction of squeezing intensity represents one of the most difficult challenges when tunnelling through squeezing ground. A timely prediction of the conditions ahead of the face would enable adjustments to be made to the temporary support, excavation diameter and final lining during construction. A number of authors have therefore attempted to identify early indicators of ground quality on the basis of field measurements. Steindorfer (1998) proposed a method of predicting changes in rock mass quality ahead of the face based on the displacement vector orientations obtained by geodetic measurements in the tunnel. Jeon et al. (2005) underpinned the method theoretically by means of numerical computations, but pointed out that it is very difficult to make a prediction under complex geological conditions. Sellner (2000) proposed a method of predicting the displacement of the tunnel boundary based on Sulem et al. (1987). This method requires an estimation to be made of the ground convergences ahead of the face, however, and this can be done only by estimating the parameters of the function defined by Sulem et al. (1987) on the basis of experiences.

Despite improvements in the theoretical assessment of the squeezing phenomenon, and despite the experiences gained with different construction methods, there are still no reliable methods of prediction available.

The analysis of deformation measurements in the ground ahead of the face looks promising with regard to ground response predictions, as the radial loading and axial deformation of the core ahead of the face can be seen as a large scale in situ test.

Figure 1 shows the mechanism leading to face extrusion schematically. The ground core ahead of the face loses its axial confinement as the tunnel face approaches. The loss of confinement reduces the radial resistance of the ground core, and the core thus deforms due to the radial load σ_r exerted by the surrounding ground. In squeezing ground, the core yields under the radial loading and extrudes into the opening. The magnitude of the extrusion depends on the mechanical properties of the ground, the depth of cover and the support measures applied at the tunnel circumference and at the tunnel face. If the ground exhibits a
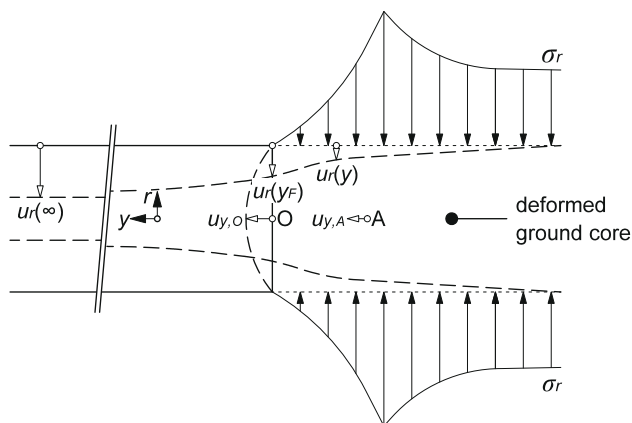
Fig. 1 Schematic mechanism of core extrusion

time-dependent behaviour (due either to creep or to consolidation), the magnitude of the extrusion will also depend on the advance rate and on the duration of any standstills.

In the past, extrusion measurements have been mostly used to control face stability. Lunardi (1995) first used such measurements in squeezing ground for the assessment both of face stability and the expected convergences. The Pianoro tunnel (Lunardi and Gatti 2010) is one recent case history showing a correlation between extrusions, convergences and the overburden.

The extrusion of the face during a standstill in squeezing ground can be from several centimetres to decimetres (cf. Cantieni and Anagnostou 2011), but it is not problematic in conventional tunnelling as long as the face remains stable (Kovári 1998). In TBM tunnelling, the excavation speed is normally high enough to avoid jamming of the cutter head during regular TBM operation, as the extruding ground is excavated as part of the boring process. Immobilization may, however, occur during a standstill (Ramoni and Anagnostou 2010). Extreme extrusions have been observed, e.g., during the construction of the Gilgel Gibe II Tunnel in Ethiopia. After encountering a fault zone, the face extruded very quickly (40–60 mm/h), and pushed back the TBM for about 60 cm (De Biase et al. 2009).

The present paper investigates the possibility of predicting the ground response to tunnelling by assessing the axial extrusion of the core ahead of the face. The paper starts with a review of the analytical, empirical and numerical approaches proposed in the literature for the quantitative assessment of core extrusion (Sect. 2). Section 3 briefly sets out the methods for monitoring extrusion, discusses some aspects of data processing and reviews monitoring results from case histories found in the literature. Section 4 investigates theoretically, by means of numerical analyses, the possibility of using extrusion data as an early indicator of tunnel convergence. Finally, extrusion and convergence measurements from the

Gotthard Base Tunnel are presented and discussed in detail with regard to the predictability of ground response (Sect. 5).

2 Computational Methods for Estimating Extrusion

Based on a spherical model of the tunnel face (Egger 1980) and on undrained ground behaviour, Mair (2008) introduced so-called "influence lines", which show the increase in axial displacement of a point ahead of the face due to the advancing face. Wong et al. (2000a) proposed spherical models for the determination of face extrusions, incorporating the effect of face reinforcement using bolts. However, the extrusions determined through laboratory experiments could not be reproduced by the analytical solution (Trompille 2003). Analytical approaches may allow a fast assessment to be made of extrusions, but the numerous simplifications (e.g. spherical face, disregard of the actual stress state) limit their predictive power.

Lunardi (2000) proposed a relation between extrusion and the radial displacements that occur ahead of the face (so-called pre-convergences), based on a volume balance of the ground ahead of the face (neglecting the dilatancy that often accompanies plastic yielding). The determination of the pre-convergences allowed him to calibrate the ground response curve and thus estimate the final lining loading by means of the convergence confinement method.

Hoek (2001) presented an approach obtained by curve-fitting the numerical results for the axial and tangential strains. In the case of an unsupported tunnel, the equations lead to a constant ratio of 1.5 between the tangential and the axial strains. Lee and Rowe (1990) presented, also based on numerical computations, a relationship between the extrusion of the face and the face support pressure for a tunnel with a rigid lining up to the face.

Kovári and Lunardi (2000) and Bernaud et al. (2009) investigated the influence of face bolting on the extrusion of the face by means of axisymmetric numerical computations. Peila (1994) and Oreste et al. (2004) investigated the deformation behaviour and face stability of shallow and deep tunnels, respectively, by means of three-dimensional numerical models. The face reinforcement was modelled with horizontal pipes embedded in the ground ahead of the face.

The ground may respond faster or slower to tunnel excavation, depending on its rheological properties. Slow ground response may reduce the extrusion of the core significantly, thus making it difficult to predict squeezing intensity (Barla 2009). The time-dependency of ground behaviour in squeezing ground can be traced back to two mechanisms: consolidation and creep (cf. Anagnostou and

Kovári 2005). Ghaboussi and Gioda (1977) showed by means of numerical computations for a visco-elastic ground behaviour that the radial displacements of the ground ahead of the face depend (among other parameters) both on the advance rate and on the viscosity of the ground. Myer et al. (1981) illustrated the effect of the advance rate on the axial strain ahead of the face by means of physical models. According to their experimental results, the faster the advance, the smaller the extrusion of one and the same material will be. A comprehensive spatial numerical investigation for a tunnel advance in visco-plastic ground was carried-out by Bernaud (1991). Pellet et al. (2009) noticed substantial face extrusion when using Lemaitre's visco-plastic damage model. Anagnostou (2007b) showed for the case of a water bearing, low permeability ground that the extrusion of the tunnel face depends on the permeability and on the advance rate (all other parameters remaining constant).

3 Extrusion Measurements

3.1 Measurement Methods

The axial deformations of the ground ahead of the face are monitored usually by means of sliding micrometers (Kovári et al. 1979). The sliding micrometer allows high precision measurements of the strain distribution along a line ahead of the face with a resolution of 1 m intervals. The main disadvantage of the sliding micrometer is the time-consuming measuring procedure, which interferes with excavation work at the face (Steiner and Yeatman 2009). The sliding micrometer has been applied successfully under both non-squeezing and squeezing conditions (e.g. Lunardi and Focaracci 1999). As experienced in the Gotthard Base Tunnel (in the northern intermediate Tavetsch formation), however, its application may be problematic under heavy squeezing conditions (damaged due high water or rock pressure; Thut et al. 2006).

A recent development that resolves the above-mentioned problems is the so-called reverse-head-extensometer (RH-extensometer) (Thut et al. 2006; Steiner 2007). In contrast to the normal extensometers (which are used for measuring the radial displacements of the ground in tunnelling), the measuring head of the RH-extensometer, which includes the data logger, is installed at the end of a borehole far ahead of the face, thus allowing a continuous monitoring of deformations with little obstruction to the excavation work (Fig. 2a). The communication cable which is used for data readout is located in a central tube and can be accessed at the face (Steiner and Yeatman 2009).
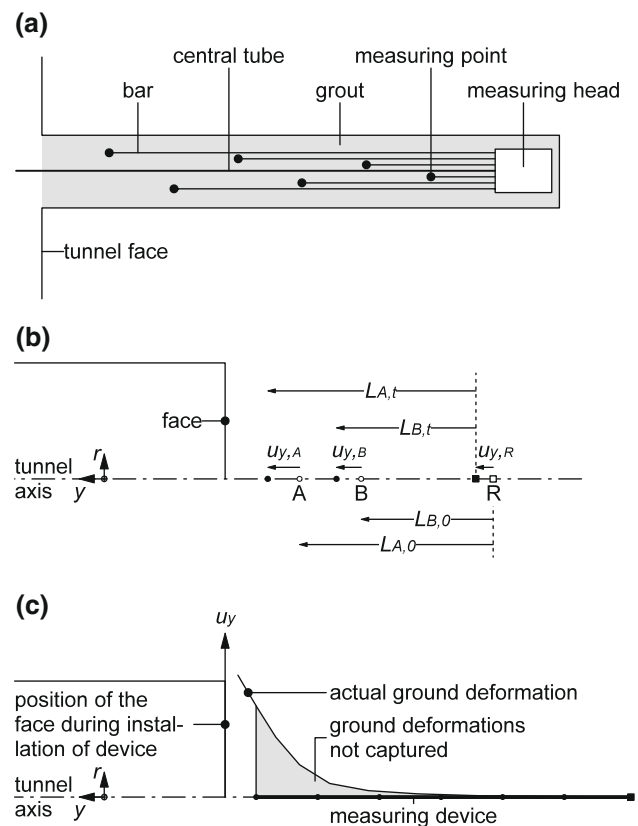

Fig. 2 a Scheme of the RH-extensometer (after Thut et al. 2006); b "Non-fixed reference point" limitation; c limitation concerning the "zero reading"

The data recorded by means of sliding micrometers or extensometers ahead of the face require careful processing to avoid erroneous results. Two sources of error will be discussed in the next section.

3.2 Data Processing

The interpretation of the monitoring data should account for the effects (1) of the reference point displacement and, (2), of the zero reading (Fig. 2b, c, respectively).

Sliding micrometers measure the length changes of the intervals defined by the successive measuring points. As discussed by Kovári (1998), Wong et al. (2000b) and Trompille (2003), the total displacements of the measuring points (e.g., the displacement $u_{y,A}$ of point A) can be determined by summing the length changes of the successive intervals, provided that the displacement $u_{y,R}$ of the reference point (which is located at the deepest point of the borehole) is known (e.g. by measuring it independently with an overlapping measuring device) or it can be assumed to be practically zero (which is true only if it is located outside the influence zone of the advancing tunnel face):

$$u_{y,\text{A}} = \Delta L_{\text{A},t} + u_{y,\text{R}}, \tag{1}$$

where $\Delta L_{\text{A},t}$ denotes the sum of the length changes of the intervals between the point A and the reference point R. Similar remarks apply to RH-extensometers, the only difference being that these instruments measure directly the length change of the intervals defined by the measuring points (e.g. point A) and the reference point R.

The uncertainties associated with a non-fixed reference point are irrelevant for the distribution of the axial strain ε_y. An interpretation of the observed behaviour in terms of strain ε_y (rather than in terms of displacement) is, therefore, advantageous, and provides a better picture of the ground. The sliding micrometers measure the length changes of successive 1 m long intervals, thus leading directly to the strain distribution along the measuring line. In the case of RH-extensometers, the strain profile can easily be calculated from the measured length changes. The average strain $\varepsilon_{y,\text{AB}}$ over the interval defined by measuring points A and B reads as follows (Fig. 3a):

$$\varepsilon_{y,\text{AB}} = \frac{\Delta L_{\text{A},t} - \Delta L_{\text{B},t}}{y_\text{A} - y_\text{B}}. \tag{2}$$

A further limitation is imposed by the time and location of the zero reading (Fig. 2c). If the measuring device is installed too close to the face (i.e. within its influence zone) the measured data will apply only to the changes in extrusion taking place after the installation of the measuring device (Lunardi and Focaracci 1999).

The effects mentioned reduce the length of the measuring line that can be used for the assessment of ground displacements considerably. As discussed by Wong et al. (2000b), in the case of one single measuring device installed right at the face, the affected length of the measuring line amounts to two times the influence length of the tunnel face. The "non-fixed reference point" and the "zero reading" effects can be avoided by an appropriate arrangement of the measuring lines or by a specific way of analysing the data.

The problem concerning the displacement of the reference point can be by-passed either by installing a series of

Fig. 3 **a** Definition of the axial displacement u_y and strain ε_y; **b** Definition of the increase in axial displacement Δu_y and in strain $\Delta \varepsilon_y$ due to a face advance by S
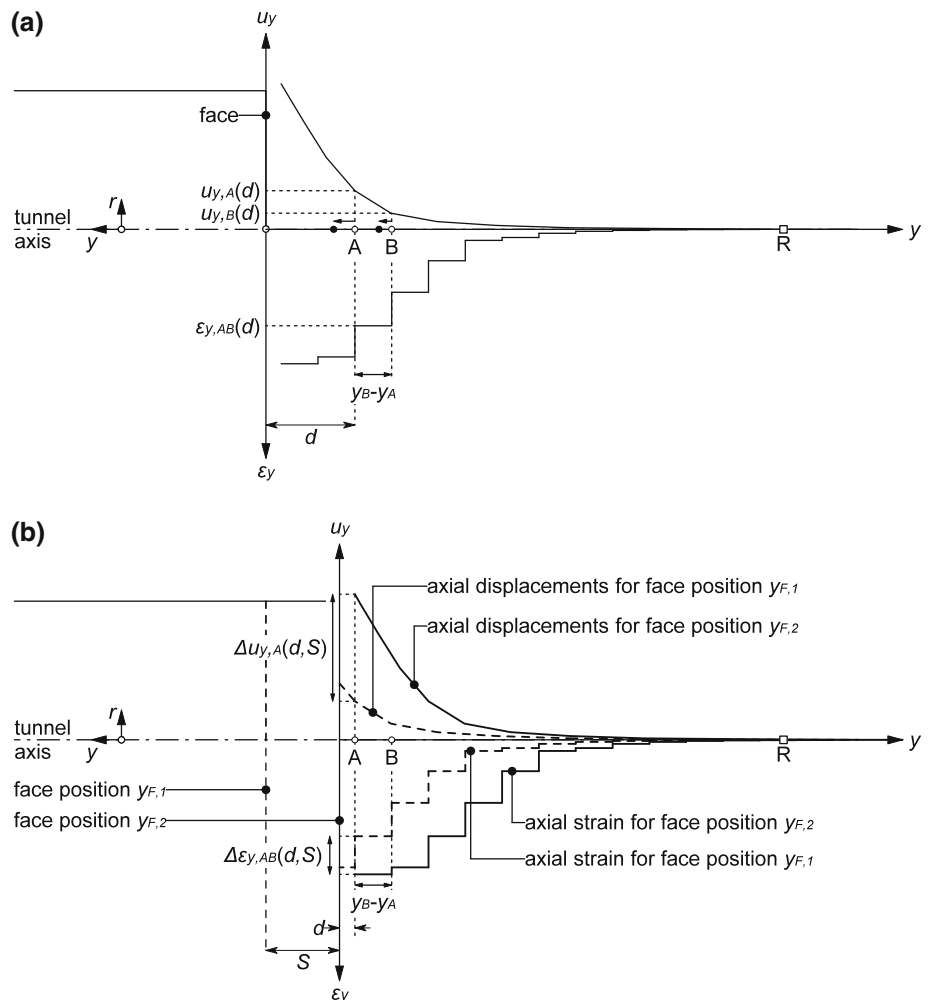
extensometers with sufficient overlapping lengths (Steiner and Yeatman 2009) or by analysing the axial strains ε_y rather than the axial displacements u_y.

The "zero reading" effect can be avoided by installing the extensometer a sufficient distance from the face in undisturbed ground, or by installing a series of overlapping extensometers (the new extensometer must be installed before the influence zone of the advancing tunnel face reaches the reference point of the preceding extensometer). When analysing the monitored data, the error associated with a "zero reading" can also be avoided by considering the increase in axial strains $\Delta\varepsilon_y$ or the increase in displacement Δu_y (Fig. 3b) caused by a face advance of S (rather than considering the total response of the ground to tunnelling).

3.3 Case Histories

Extrusion measurements have been performed in a number of tunnel projects in the recent years (Table 1). Some selected cases will be discussed below.

Table 1 Tunnel projects with extrusion monitoring documented in the literature

Tunnel	References
Tartaiguille	Wong et al. (2000b, 2004)
	Wong and Trompille (2000)
	Lunardi (1999, 2008)
Raticosa	Boldini et al. (2004)
	Bonini et al. (2009)
	Lunardi and Focaracci (1999)
	Barla et al. (2004)
	Lunardi et al. (2009)
	Barla (2005)
Vasto	Lunardi and Focaracci (1997)
	Lunardi (1998)
Saint Martin La Porte access gallery (Lyon-Turin Base Tunnel)	Russo et al. (2009)
Marinasco	Barla and Barla (2004)
San Vitale	Cosciotti et al. (2001)
	Rossi (1995)
	Lunardi and Bindi (2004)
Osteria	Barla (2005)
	Barla et al. (2004)
Bois de Peu (France)	Eclaircy-Caudron et al. (2009)
Sedrun Lot of the Gotthard Base Tunnel	Steiner and Yeatman (2009)
	Steiner (2007)

3.3.1 Tartaiguille Tunnel

The Tartaiguille tunnel will be looked at as a first example. It forms part of the French high-speed railway line between Lyon and Marseilles (Paulus 1998). The tunnel was constructed between 1995 and 1998. Its length is 2,338 m and the maximum overburden amounts to 137 m. The tunnel crosses several Cretaceous formations. The section of the tunnel, which is investigated in the present paper, is located in marly clays of the so-called "lower Stampien". Figure 4a shows the geological longitudinal profile of the tunnel. The tunnel was excavated full face ($A_F = 180$ m^2) with 90 fibreglass bolts of 24 m for face reinforcement (between chainage 495 and 1,370 m). The bolts were installed every 12 m (the bottom of Fig. 4b shows the stages of face reinforcement). More detailed descriptions of the project can be found elsewhere (e.g. Lunardi 2008; Wong et al. 2000b). The extrusion of the face was monitored by sliding micrometers. The present case study discusses the extrusions between chainage 1,251 and 1,215 m (rectangle in Fig. 4a). The excavation advances in the direction of the decreasing chainage.

Figure 4b shows the axial displacement assuming a fixed reference point and the longitudinal section of the tunnel at the position of the installation of the sliding micrometer. Additionally, the figure also shows the cross section of the tunnel. The maximum extrusion u_y at the face increases for the first six readings and remains constant afterwards. Figure 4c shows the so-called influence lines of the axial displacements u_y (assuming a fixed reference point). They show, analogously to the influence lines known from structural engineering, the axial deformation u_y (or strain ε_y) of a point in the function of its distance d to the approaching face. According to Wong et al. (2000b), the first 15 measuring points (the upper diagram of Fig. 4c) and the last 15 (the lower diagram of Fig. 4c) measuring points do not show the correct displacements u_y profile of the ground, due to the "zero reading" effect and to the "fixed reference point" effect, respectively (cf. Sect. 3.2) and, therefore, cannot be used for data interpretation.

As discussed in Sect. 3.2, the "fixed reference point" effect can be avoided by analysing the axial strains ε_y and not the axial displacements u_y. Figure 4d shows the influence lines of the axial strain ε_y. Such an illustration makes it possible to incorporate the measuring points between chainage $y = 1,229$ m and $y = 1,215$ m (the lower diagram of Fig. 4d) in the analysis.

The influence lines of Fig. 4d show that the ground response to excavation is variable. The measuring points 1,223, 1,225, 1,227, 1,229 and 1,231, for instance, show a high increase in the strain for the advance from 5 to 3 m, and a subsequent decrease in the strain for the advance from 3 to 1 m. This expansion and subsequent
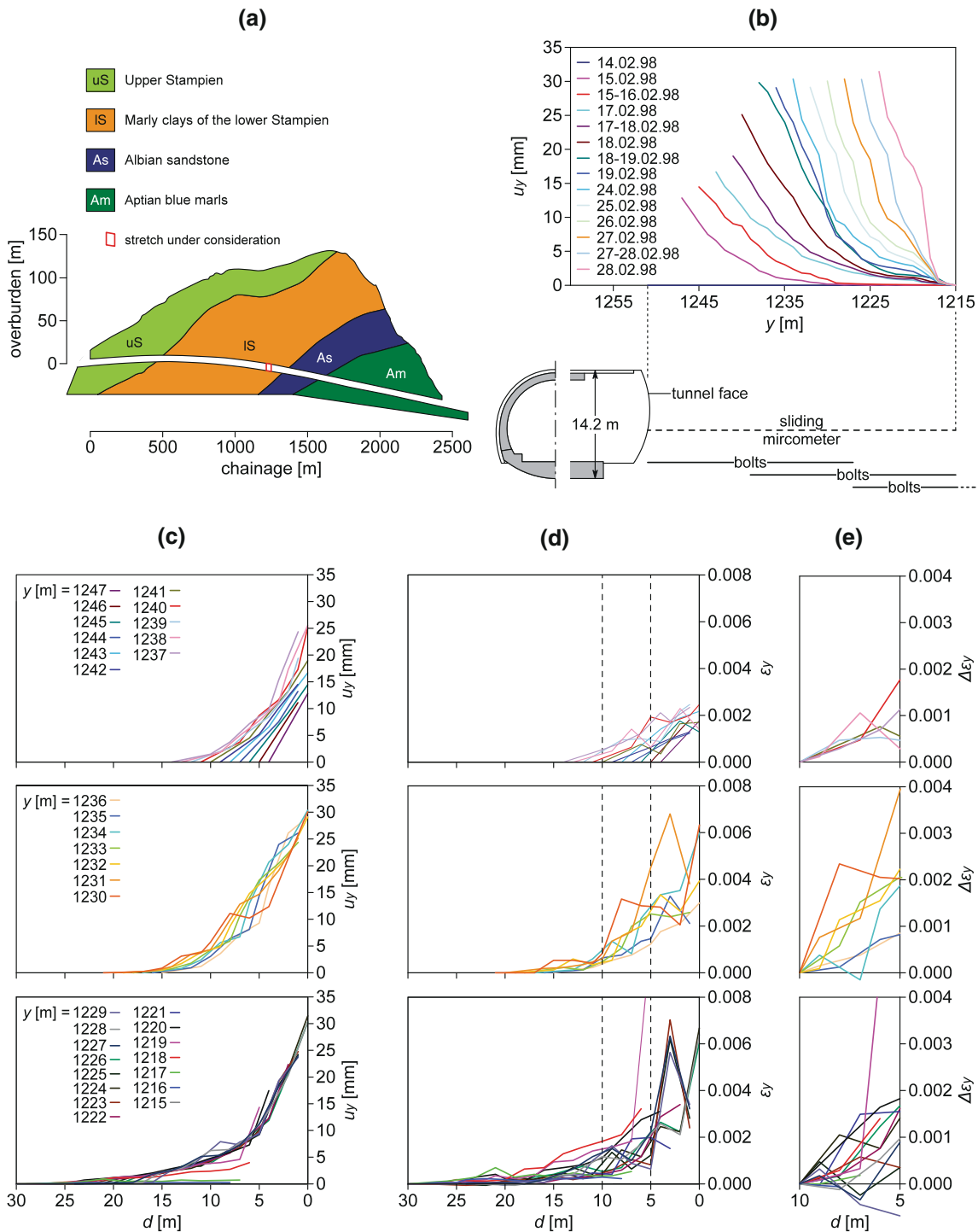
Fig. 4 a Longitudinal geological profile of the Tartaiguille tunnel (after Wong and Trompille 2000) and tunnel stretch under consideration (*rectangle*); **b** Axial displacement u_y as a function of the chainage y for different dates and positions of the face y_F (after Wong et al. 2000b) (the chainage of the first value of the extrusion u_y corresponds to the position of the face) as well as longitudinal and cross section of the tunnel (after Lunardi 1999); **c** influence line of the axial displacements u_y of the measuring points (the notation of the measuring points denotes their y-coordinates); **d** axial strain ε_y of the ground between the measuring points as a function of their distance to the face d; **e** influence line of the change in axial strain ε_y caused by the face approaching from a distance of 10 m to a distance of 5 m

recompression of the ground may be caused by a heterogeneous rock structure (layers of different ground quality perpendicular to the tunnel axis).

An analysis of the change in strain $\Delta\varepsilon_y$ due to a specific face advance makes it possible to incorporate and compare all measuring points (cf. Sect. 3.2). The curves between the

vertical dashed lines in Fig. 4d define the strain portion generated during the face advance from $d = 10$ m to $d = 5$ m for every ground interval ahead of the face. By comparing these strain portions (Fig. 4e), different behaviours of the core can be distinguished. The strain $\Delta\varepsilon_y$ developed during the face advance of 5 m amounts to about 0.001 for the intervals up to $y = 1{,}235$ m. In the subsequent intervals $y = 1{,}234, 1{,}233, 1{,}232, 1{,}230, 1{,}226, 1{,}224, 1{,}222, 1{,}221, 1{,}220$ and $1{,}218$ m, the strain increases to about 0.002. There seems to be a change either in ground quality or in support measures after chainage $y = 1{,}235$ m, causing an increase in extrusion ahead of the face. Some of the intervals especially in the lower diagram of Fig. 4e even show a decrease in strain due to a face advance (e.g. $y = 1{,}229$ m). This behaviour may be caused, as already mentioned above, by rock structure heterogeneities.

3.3.2 Raticosa Tunnel

The Raticosa tunnel is part of the Bologna to Florence high-speed railway line, which crosses the Apennine range (Lunardi and Focaracci 1999). The tunnel has a length of about 10.5 km and the maximum overburden is about 500 m. The section under investigation is located near the northern portal and was excavated full face ($A_F = 160$ m^2) in 1998 (Fig. 5a). The tunnel was excavated from the northern portal through a landslide area, formed of intensely tectonised clay shales (Bonini et al. 2009). The overburden ranged from a few meters to 100 m. The face was reinforced with 60 fibre-glass bolts, which had a length of 20 m and were installed every 10 m of face advance. After excavating, in steps of about 1.5 m, steel sets (at 1 m spacings) and shotcrete were applied. The final lining invert was cast within a distance of about one tunnel diameter from the face. The final concrete lining was completed in a distance of about 30–40 m behind the face. The extrusion of the face was monitored with a sliding micrometer of 30 m length. Only six extrusion measurements are available (including the zero reading).

Figure 5b shows the construction sequence, the axial displacement profile assuming a fixed reference point as well as the longitudinal section and cross section of the tunnel. A break from the 6th to the 15th July 1998 at face position 10 m and a subsequent face advance from 10 to 12 m generated a major extrusion (Fig. 5b). The extrusion probably developed over time during the standstill. Note, furthermore, that the subsequent face advance from 12 to 15 m caused only very limited deformations. The installation of heavy face reinforcement during the break could be the reason for the limited axial displacements. The lack of information regarding the executed sequence of face support installation makes it impossible to verify this conclusion.

According to the reading of the 4th July 1998 (face position at 6 m) the zone of influence is about 19 m (Fig. 5b). The large zone of influence is evident also in Fig. 5c, which shows the influence lines of the axial displacements u_y (assuming a fixed reference point). The total value of the extrusion u_y cannot be determined for most of the points, because the zero reading was done when the ground had already experienced deformations (note the influence zone extends up to 18–19 m ahead of the face!) and because the records for the face advance after $y_F = 14.8$ m are missing.

According to the definition of Wong et al. (2000b), the usable length of this extensometer is reduced to zero. However, if we take account of the strains (instead of the displacements), more data can be used (cf. Sect. 3.2). Figure 5d shows the influence lines of the strains ε_y. A comparison of the increase in strains does not yield more information because there are no readings after face position of $y_F = 15$ m. A detailed interpretation of the data is very difficult because there are only a few readings. It is, therefore, possible to recognize only pronounced changes in extrusion.

The convergences were monitored at two cross sections (denoted by "a" and "b" in Fig. 5b). Figure 5e shows the convergences u_c measured between the measuring points 1 and 5 at these two cross sections as a function of the distance from the face d_c. Both cross sections show approximately the same development of the convergences. The convergences stabilize (at about 40 mm only) after the installation of the invert (Bonini 2003). As shown later in Sect. 4 by means of numerical calculations, the extrusion does not provide any useful indication as to the convergence in case of stiff linings which are installed close to the face, because in such cases the convergences are almost independent of the ground quality.

3.3.3 Vasto Tunnel

The Vasto tunnel is part of the railway line from Ancona to Bari. The tunnel has a length of about 6.2 km and maximum overburden of 135 m. The main part of the tunnel crosses complex formations consisting of a silty, clayey constitution, stratified with thin sandy intercalations and containing sizeable water bearing sand lenses. The excavation work began in 1983 and was stopped after several incidences in 1990. In 1992 the work continued with a new design concept, which also incorporated extrusion measurements. The tunnel was excavated full-face ($A_F \approx 120$ m^2). The face was reinforced by 55 fibre-glass bolts and horizontal jet-grouting was performed in advance around the future tunnel (Lunardi and Bindi 2004). A detailed description of the project can be found in Lunardi and Focaracci (1997).
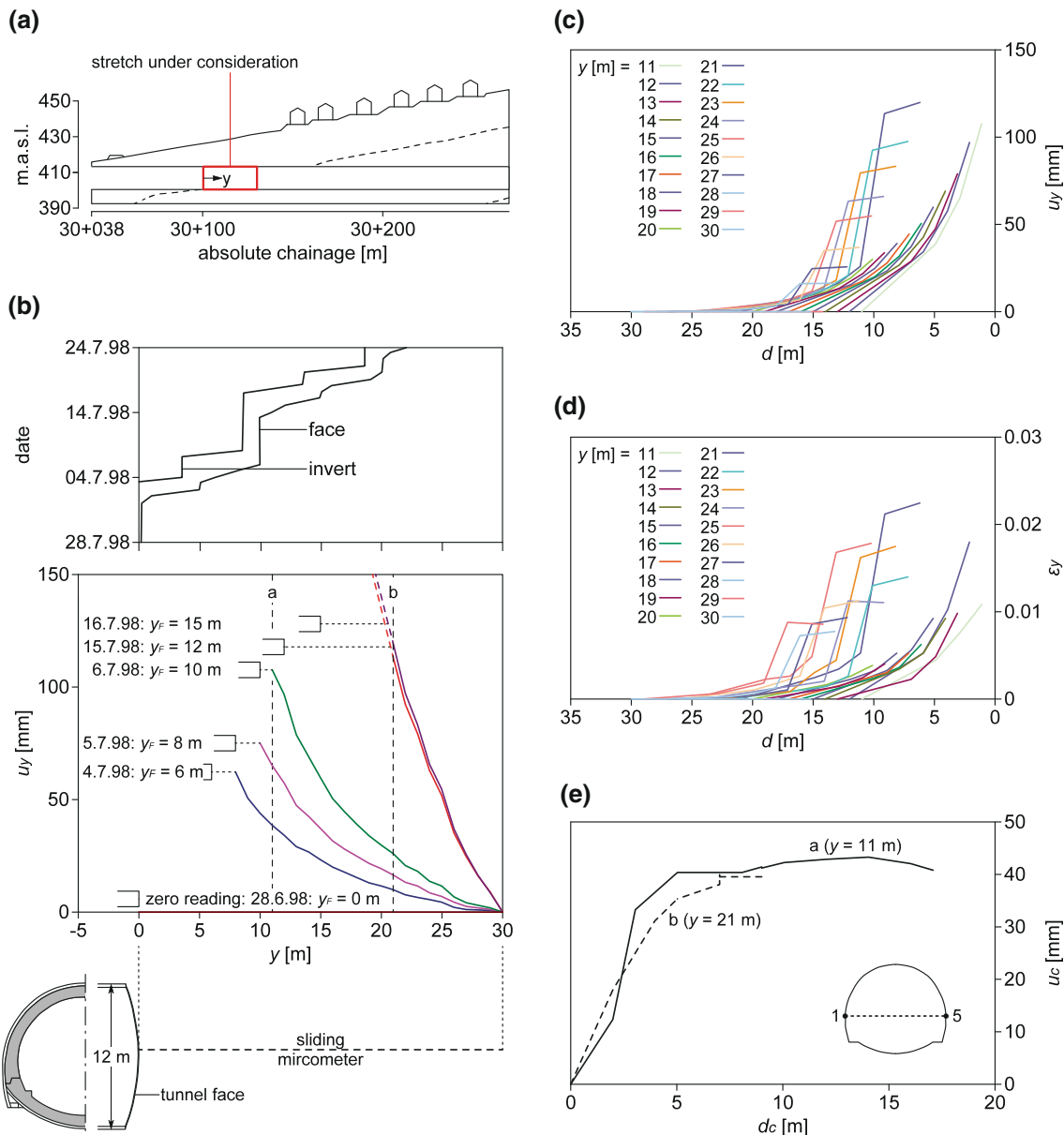
(a)

(b)

(c)

(d)

(e)

Fig. 5 **a** Longitudinal geological profile of the Raticosa tunnel (after Lunardi and Focaracci 1999) with the tunnel stretch under consideration (*rectangle*); **b** construction sequence, distribution of the axial displacement u_y as a function of the chainage y ($y = 0$ corresponds to the absolute chainage of $30 + 102$) for different dates (and positions of the face y_F) (after Bonini et al. 2009) as well as longitudinal and cross section of the tunnel (after Boldini et al. 2004); **c** axial displacements u_y of the measuring points as a function of their distance to the face d; **d** influence lines of the axial strain ε_y (the notation of the intervals denotes the y-coordinate of their first points); **e** Influence lines of convergences at the chainages $30 + 113$ m ($y = 11$ m) and $30 + 123$ m ($y = 21$ m)

Figure 6a shows the longitudinal profile of the tunnel and the approximate location of the monitored stretch. Both extrusion- and convergence-measurements are available for this tunnel. Figure 6b shows the cross section and the longitudinal section of the tunnel (including the axial sliding micrometer and the location of convergence measurements a, b, and c) and the extrusion profiles assuming a fixed reference point recorded during face advance. After the excavation passed chainage $y = 3$ m, the extrusion profiles show a considerable increase in displacement. Furthermore, it is remarkable that, on the one hand, the maximum extrusions of the first three recordings (the curves for $y_F = 1$, 2 or 3 m) are relatively small, but on the other hand the profiles indicate a very large influence zone of the face (extending up to 15–20 m ahead of the face). The large zone of influence can also be seen in Fig. 6c, which shows the influence lines of the axial displacements u_y (assuming a fixed reference point). However,

the influence lines of the axial strain ε_y indicate a much smaller influence zone (about 9 m, Fig. 6d). A closer examination of the extrusion profiles confirms this conclusion (the distances of the measuring points far ahead of the face remain practically constant - the displacement profiles are practically horizontal). The difference between the zone of influence indicated by the displacements and by the strains is probably due to the measuring inaccuracies.

The convergences were monitored at three cross sections (denoted by a, b and c in Fig. 6b). Figure 6e shows

the convergences u_c measured at these three cross sections as a function of the distance from the face. The convergences at the chainages $y = 3$ m (point b) and $y = 6$ m (point c) increased after the face passed chainage $y = 8$ m. According to Lunardi and Focaracci (1997), these results indicate that a high face support reduces both the extrusion and the convergences. As shown later in Sect. 4 by means of numerical calculations, a lighter face support should lead theoretically to bigger extrusions (particularly in the case of a low overburden) but smaller convergences. The
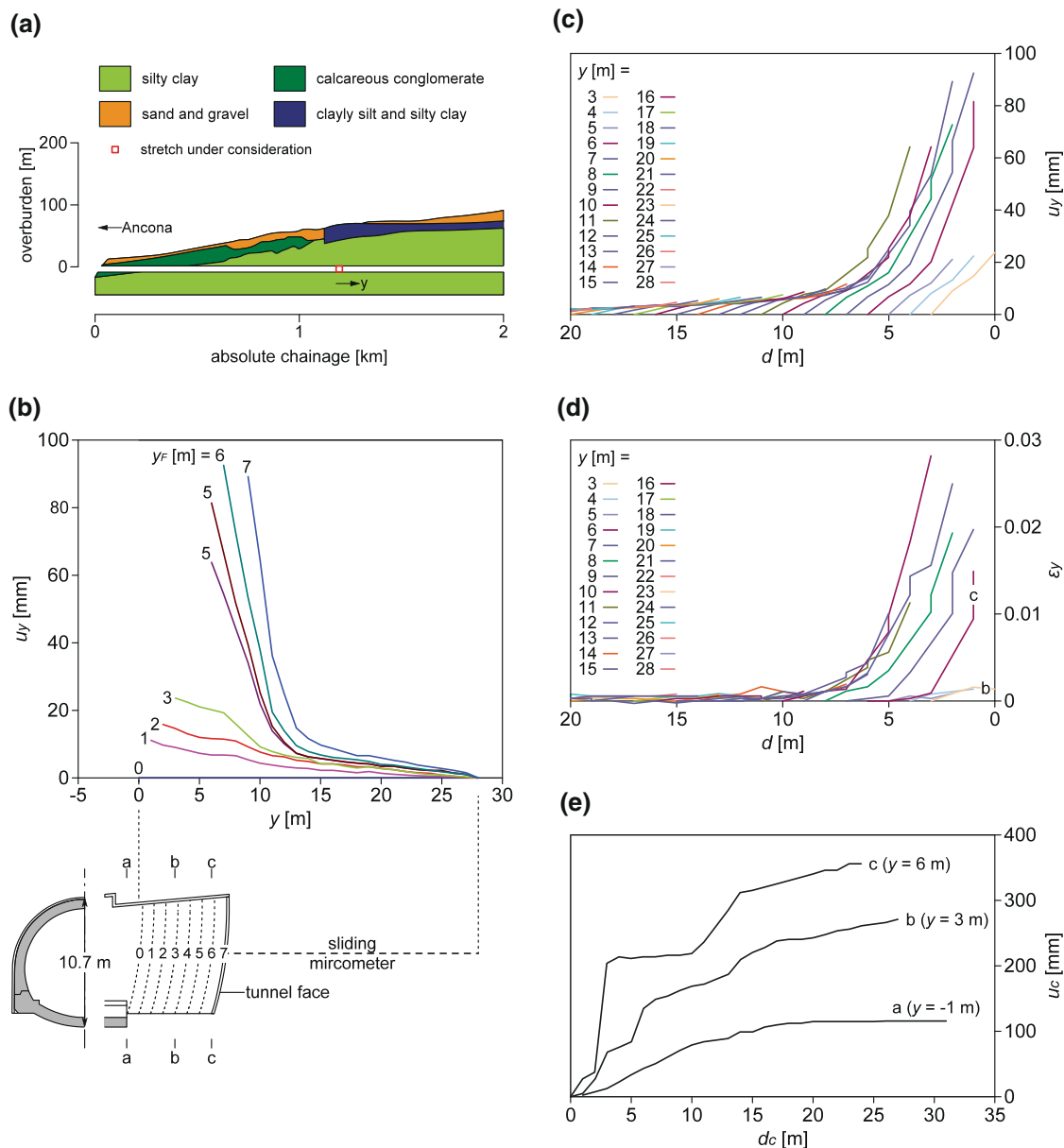

Fig. 6 a Longitudinal geological profile of the Vasto tunnel (after Lunardi 2000) and stretch under consideration (*rectangle*); **b** axial displacement u_y as a function of the chainage y for different positions of the face y_F (Lunardi and Focaracci 1997) as well as longitudinal and cross section of the tunnel (after Lunardi 2000); **c** influence lines of axial displacements u_y of a measuring point at chainage y; **d** influence lines of axial strain ε_y over the intervals between the measuring points at chainage y and $(y + 1$ m); **e** influence lines of convergences at the chainages $y = -1$, 3 and 6 m

data documented in the literature are not sufficient for establishing the reason for the observed increase in convergences with certainty. The large convergences monitored (>0.3 m) indicate that the lining was not installed immediately behind the face. An increase in the distance between the face and the lining installation (or a decreasing ground quality after chainage $y = 8$ m) would also lead to larger convergences. However, the monitored data show a weak correlation between the extrusions and the convergences.

4 Theoretical Aspects

4.1 Introduction

The present section analyses the response of the core ahead of the face numerically to gain a better understanding of the observed behaviour, and to investigate whether there is a correlation between extrusions and convergences. The numerical analyses take into account the effects of support (face support, yielding support or stiff support) and ground properties (e.g. strength, deformability, rheology and heterogeneity). As a reference point, the case of an unsupported tunnel crossing a homogeneous ground with time-independent behaviour will be discussed first.

4.2 An Unsupported Tunnel in Homogeneous Ground

4.2.1 Numerical Model

For the numerical analysis of the deformation behaviour of the core ahead of the face, an axisymmetric model of a deep, unsupported, cylindrical tunnel crossing a homogeneous and isotropic ground which is subject to uniform and hydrostatic initial stress will be considered (Fig. 7). The mechanical behaviour of the ground is modelled as linearly elastic and perfectly plastic according to the Mohr–Coulomb yield criterion, with a non-associated flow rule. The angle of dilatancy ψ was taken equal to $\varphi - 20°$ for $\varphi > 20°$ and to $0°$ for $\varphi \le 20°$ (cf. Vermeer and de Borst
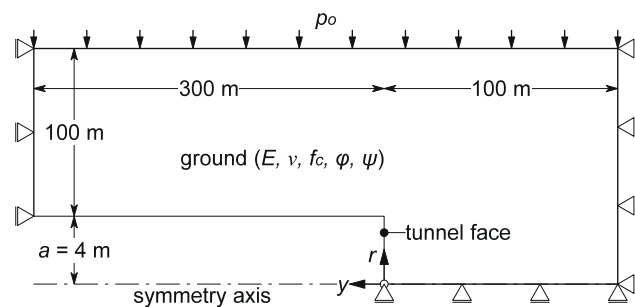

Fig. 7 Axisymmetric model and boundary conditions

Table 2 Model parameters

Parameter		Value
Initial stress	p_0	10 MPa
Tunnel radius	a	4 m
Ground		
Young's Modulus	E	1 GPa
Poisson's ratio	v	0.3
Angle of internal friction	φ	variable
Dilatancy angle	ψ	$\varphi - 20°$ for $\varphi > 20°$; $0°$ for $\varphi \le 20°$
Uniaxial compressive strength	f_c	variable

1984). According to comparative calculations, the angle of dilatancy does not affect the relationship between the extrusions and the convergences significantly, because an increase of the angle of dilatancy will increase both the extrusions and the convergences. Table 2 summarizes the parameters of the model. Normalized uniaxial compressive strengths f_c/p_0 of down to 0.05 have been considered in the numerical computations. Such low values represent very heavily squeezing conditions which have, for instance, been encountered at the Sedrun Lot of the Gotthard Base Tunnel (cf. Sect. 5.2). The numerical solution of the axisymmetric tunnel problem has been obtained by means of the finite element method. The problem is solved numerically by the so-called "steady state method", a method introduced by Nguyen-Minh and Corbetta (1991) for efficiently solving problems with constant conditions in the tunnelling direction by considering a reference frame which is fixed to the advancing tunnel face. A comparison of the steady state method with the more widely used step-by-step method, which handles the advancing face by deactivating and activating the ground and support elements respectively, can be found in Cantieni and Anagnostou (2009a).

To save computation and data processing time, some general properties of the solutions of elasto-plastic tunnel problems will be taken into account in the numerical analyses. The displacement u of the boundary of an unsupported opening in linearly elastic (according to Hooke's law) and perfectly plastic ground (obeying the Mohr–Coulomb yield criterion and a non-associated flow rule) depends on the material constants of the ground (E, v, f_c, φ, ψ), on the initial stress p_0 and on the problem geometry (in the present case the tunnel radius a of the cylindrical tunnel):

$$u = f_1(E, \ v, \ f_c, \ \varphi, \ \psi, \ p_0, \ a). \tag{3}$$

The parameters can be reduced by means of a dimensional analysis and by normalizing the displacements by the reciprocal value of the Young's modulus E (c.f. Anagnostou and Kovári 1993):

$$\frac{uE}{ap_0} = f_2\left(v, \ \varphi, \ \psi, \ \frac{f_c}{p_0}\right). \tag{4}$$

With reference to the spatial model of an advancing tunnel, both the radial displacements at the tunnel face $u_r(y_F)$ (Fig. 1) and the final radial displacements far behind the face $u_r(\infty)$ can be expressed by Eq. 4:

$$\frac{u_r(y_F)E}{ap_0} = f_3\left(v, \ \varphi, \ \psi, \ \frac{f_c}{p_0}\right), \tag{5}$$

$$\frac{u_r(\infty)E}{ap_0} = f_4\left(v, \ \varphi, \ \psi, \ \frac{f_c}{p_0}\right). \tag{6}$$

The convergence of the opening u_c is according to Eq. 5 and 6:

$$\frac{u_c}{ap_0}E = \frac{u_r(\infty) - u_r(y_F)}{ap_0}E = f_4 - f_3 = f_5\left(v, \ \varphi, \ \psi, \ \frac{f_c}{p_0}\right). \tag{7}$$

The axial displacement u_y at a location y can be expressed as:

$$\frac{u_y E}{ap_0} = f_6\left(v, \ \varphi, \ \psi, \ \frac{f_c}{p_0}, \frac{y}{a}\right). \tag{8}$$

The axial strains ε_y at the tunnel axis are obtained as:

$$\varepsilon_y = \frac{\partial u_y}{\partial y} = a\frac{p_0}{E}\frac{\partial f_6\left(v, \ \varphi, \ \psi, \ \frac{f_c}{p_0}, \frac{y}{a}\right)}{\partial y}$$
$$= \frac{p_0}{E}f_7\left(v, \ \varphi, \ \psi, \ \frac{f_c}{p_0}, \frac{y}{a}\right). \tag{9}$$

The change in axial strain $\Delta\varepsilon_y$ at any location due to a face advance of S can be expressed by a similar equation (cf. Figure 3b):

$$\Delta\varepsilon_y\frac{E}{p_0} = f_8\left(v, \ \varphi, \ \psi, \ \frac{f_c}{p_0}, \frac{y}{a}, \frac{S}{a}\right). \tag{10}$$

Figure 3 shows the longitudinal profiles of the displacement u_y, strain ε_y and strain increase $\Delta\varepsilon_y$ due to a face advance of S. The indexes A and B denote points on the tunnel axis. In homogeneous ground, the absolute position on the axial co-ordinate y is not relevant, and only the distance to the face d has to be considered. The expressions for the displacements and strains can thus be simplified to: $u_y(d)$, $\varepsilon_y(d)$ and $\Delta\varepsilon_y(d, S)$.

4.2.2 Numerical Results

Deformed Shape of the Face Figure 8a shows the curved shape of the deformed face for different normalized uniaxial compressive strengths f_c/p_0. As expected, the maximum extrusion appears in the centre of the face. Figure 8b shows that the extrusion of the face $u_y(0)$ is about constant for uniaxial strengths higher than $0.8p_0$. The maximum
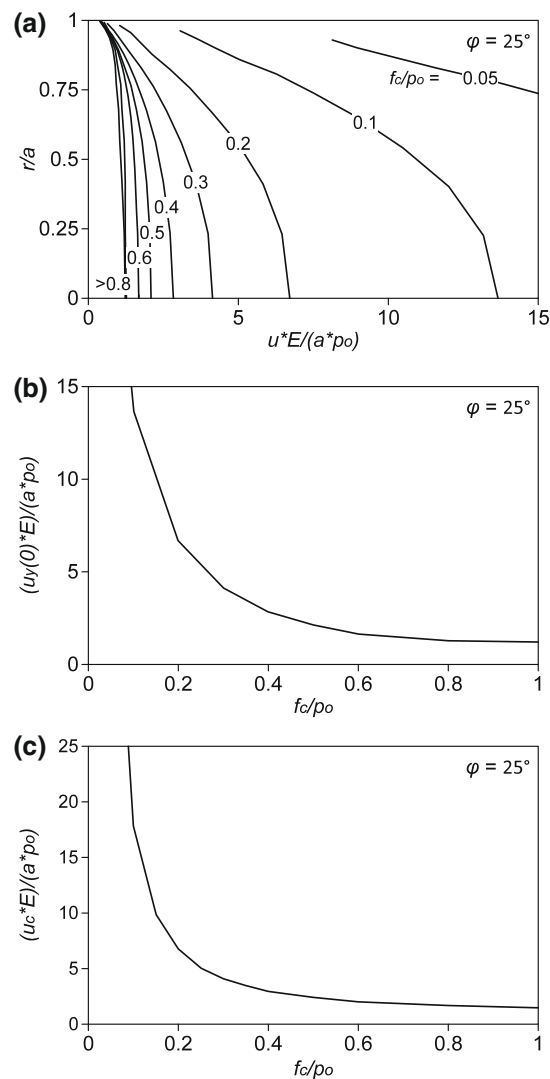

Fig. 8 Unsupported tunnel. **a** Deformed shape of the face as a function of the normalized uniaxial compressive strength f_c/p_0; **b** Normalized extrusion of the centre of the face $u_y(0)*E/(a*p_0)$ as a function of the normalized uniaxial strength f_c/p_0; **c** normalized convergences $u_c*E/(a*p_0)$ as a function of the normalized uniaxial strength f_c/p_0

extrusion increases strongly for uniaxial strengths lower than about $0.4p_0$.

Figure 8c shows the radial displacements of the tunnel boundary $u_c = u_r(\infty) - u_r(y_F)$ (cf. Figure 1) as a function of the normalized uniaxial strength f_c/p_0. The curve shows a similar development to Fig. 8b with respect to the uniaxial compressive strength of the ground, thus suggesting a strong correlation between these two variables.

Displacements and Strains Along the Tunnel Axis Figure 9a shows the axial displacements $u_y(y)$ at the tunnel axis ahead of the face (extrusion profile) for different normalized uniaxial compressive strengths f_c/p_0. Both the magnitude of the displacements and the region ahead of the face influenced by the excavation increase with decreasing

ground strength. Figure 9b shows the axial strains $\varepsilon_y(y)$ at the tunnel axis. The strain decreases with the distance y to the face. It is remarkable that the strain is constant in the region close to the face ($y < 0.25a$ to $0.5a$). This behaviour can be traced back to the arching effect ahead of the face (the centre of the face is not stressed by the surrounding ground). This behaviour also becomes evident when considering the increase in strain $\Delta\varepsilon_y(y)$ due to a face advance of $S = 1$ m (Fig. 9c). The centre of the core, at a distance of $a/4$ ahead of the face, is not influenced significantly by the face advance. The biggest increase in strain occurs at a distance y of about $0.5a$ to a ahead of the face.

In homogeneous ground the extrusion profiles of Fig. 9 are identical to the influence lines of the extrusion. The diagrams of Fig. 9 can be read as influence lines by replacing the axial coordinate y with the distance to the face d.
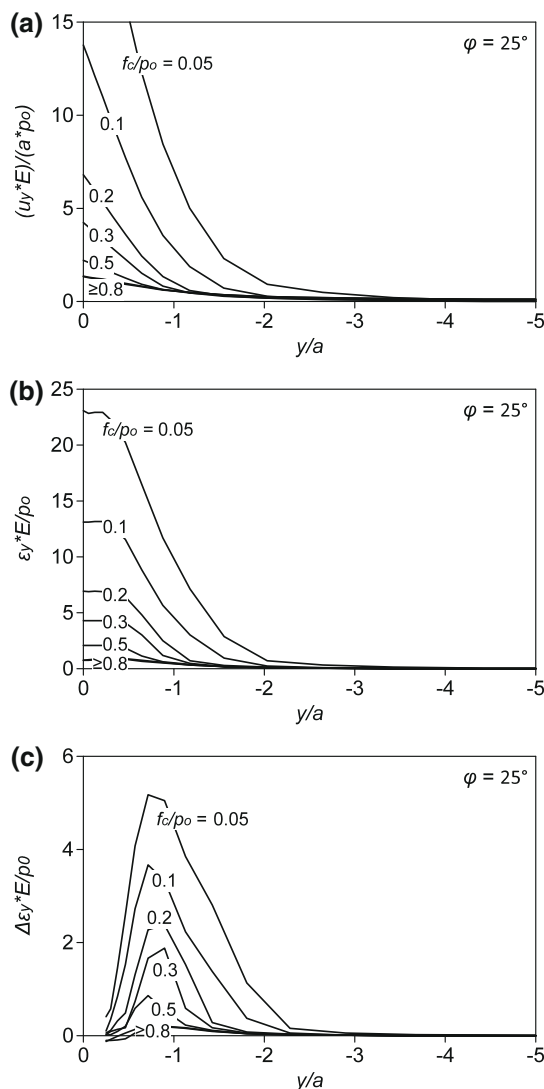
Relationship Between Extrusion and Convergences The radial displacements occurring in the tunnel can be expressed by the tangential strain which develops at the tunnel boundary behind the tunnel face:

$$\varepsilon_{t,\mathrm{c}} = \frac{u_r(\infty) - u_r(y_F)}{a}, \tag{11}$$

where $u_r(\infty)$ and $u_r(y_\mathrm{F})$ denote the final radial displacement of the ground occurring far behind the face and the radial displacement of the ground at the face, respectively.

Figure 10 shows the tangential strain $\varepsilon_{t,\mathrm{c}}$ as a function of the axial strain at the centre of the face $\varepsilon_y(0)$ for different values of the normalized uniaxial compressive strength f_c/p_0 (thin solid lines) and of the friction angle φ (thick solid lines). The conditions that lead to high axial strains at the face lead also to larger convergences of the tunnel (see Figs. 8b and 8c). As the relationship is unique, prediction is theoretically possible. The dashed lines in Fig. 10 show that most values are in the range of $\varepsilon_{t,\mathrm{c}}/\varepsilon_y(0) = 1$ to 2.

Figure 11a shows the ratio $\varepsilon_{t,\mathrm{c}}/\varepsilon_y(0)$ as a function of the normalized uniaxial compressive strength f_c/p_0. Each curve clearly consists of four sections:

I	$f_\mathrm{c}/p_0 \geq 2$
II	$0.8 < f_\mathrm{c}/p_0 < 2$
III	$0.3 < f_\mathrm{c}/p_0 < 0.8$
IV	$f_\mathrm{c}/p_0 < 0.3$

Section I, which concerns high strength to initial stress ratios, concerns elastic behaviour, and is, therefore, characterized by a constant ratio $\varepsilon_{t,\mathrm{c}}/\varepsilon_y(0)$ of about 1.75. When the uniaxial strength decreases to values lower than $f_\mathrm{c}/p_0 = 2$, plastic yielding occurs around the tunnel, while the central portion of the core ahead of the face remains in the elastic domain as long as the ratio of f_c/p_0 is higher than 0.8 (Fig. 11b). The axial strains thus remain approximately constant in section II, while the tangential strains increase

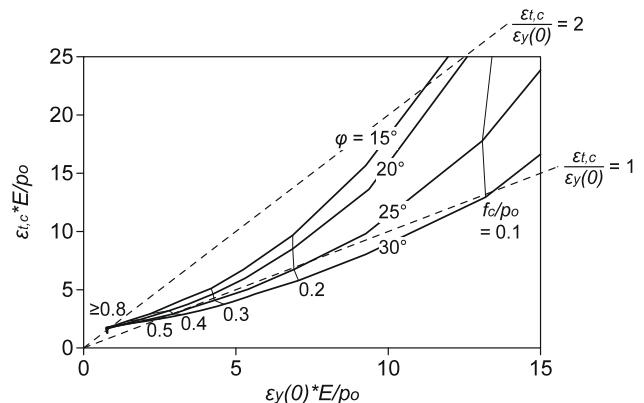**Fig. 9** Unsupported tunnel. Longitudinal distribution of **a** normalized axial displacements $u_y*E/(a*p_0)$, **b** strains ε_y*E/p_0 and **c** increase of strain $\Delta\varepsilon_y(S)*E/p_0$ caused by a face advance of $S = a/4$

Fig. 10 Unsupported tunnel. Normalized tangential strain $\varepsilon_{t,\mathrm{c}}*E/p_0$ over normalized axial strain at the centre of the face $\varepsilon_y(0)*E/p_0$
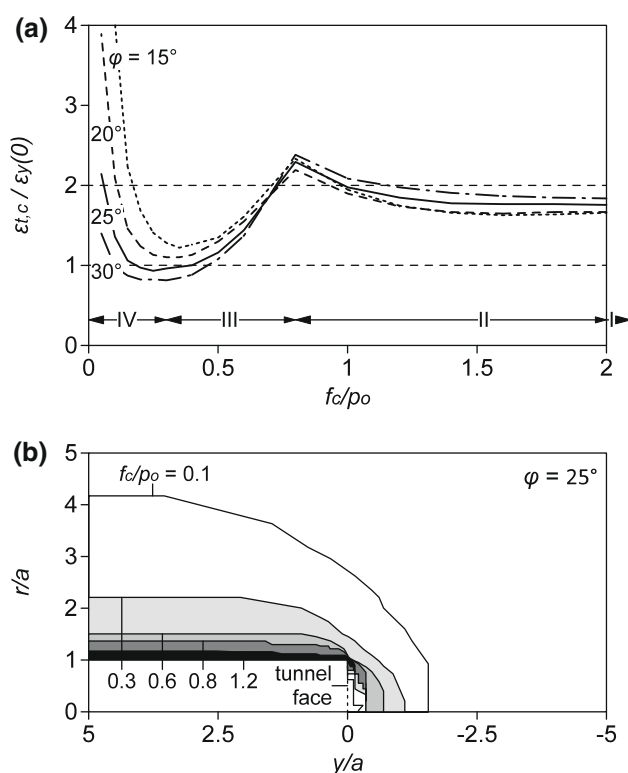
(a)

(b)

Fig. 11 Unsupported tunnel. **a** Ratio of normalized convergence to axial strain as a function of the normalized uniaxial compressive strength f_c/p_0; **b** extent of the plastic zone

with decreasing uniaxial strength. At f_c/p_0 ratios lower than $f_c/p_0 = 0.8$, the plastic zone comprises the entire core ahead of the face (Fig. 11b). The extrusion of the core is then mainly due to the developing plastic strains, which increase with decreasing ground strength (section III). In section IV, the convergence to extrusion ratio increases rapidly with decreasing compressive strength. The reason is that for $f_c/p_0 < 0.3$ the plastic zone continues to increase considerably in the radial direction around the tunnel but increases only slightly ahead of the face (Fig. 11b).

The parts mentioned above are similar to the cases distinguished by Panet (1995, 2009) using the stability coefficient $N = 2p_0/f_c$:

$f_c/p_0 > 1$	(N < 2)	No plastic zone ahead of the tunnel face
$0.4 < f_c/p_0 < 1$	(2 < N < 5)	The plastic zone comprises only part of the tunnel face
$f_c/p_0 < 0.4$	(N > 5)	Large plastic zone comprising the entire tunnel face

The dashed lines in Fig. 11a also show that most cases have a ratio $\varepsilon_{t,c}/\varepsilon_y(0)$ between 1 and 2. Only in case of very poor ground does the ratio increase to over 3. The ratio of $\varepsilon_{t,c}/\varepsilon_y(0) = 1.5$ proposed by Hoek (2001) is, therefore, a good approximation.

4.3 The Effect of a Yielding Support

Under severe squeezing conditions, yielding supports are used to reduce the rock pressure on the lining. In the present section, the yielding support is modelled in a simplified way by assigning a constant pressure (which is taken to be equal to the yield pressure p_y of the support) on the tunnel boundary. For alternative models and a detailed analysis of the interaction of yielding supports with squeezing ground see Cantieni and Anagnostou (2009b).

By introducing the normalized yielding pressure p_y/p_0 as an additional parameter in Eq. 9, the axial strains of the ground at the tunnel axis can be expressed by the following function:

$$\varepsilon_y \frac{E}{p_0} = f_9\left(v,\ \varphi,\ \psi,\ \frac{f_c}{p_0}, \frac{y}{a}, \frac{p_y}{p_0}\right). \tag{12}$$

The numerical model is identical to the model of Fig. 7, with the difference that the pressure p_y is applied as a boundary condition to the tunnel boundary (inset of Fig. 12).

The thick solid lines of Fig. 12 show the effect of the normalized yielding pressure of the support p_y/p_0 for a series of normalized uniaxial compressive strengths f_c/p_0 (thin solid lines).

According to Fig. 12, the higher the yield pressure p_y of the support, the lower will be the tangential strain $\varepsilon_{t,c}$ and the axial strain at the centre of the face $\varepsilon_y(0)$. The reduction in the tangential strain $\varepsilon_{t,c}$ is more pronounced. The curve flattens for increasing yield pressures p_y. At very high ratios of yield pressure to initial stress ($p_y > 0.1p_0$), the curve is so flat that the axial strains do not provide any indication as to the magnitude of the convergences. Such high p_y/p_0-ratios are, however, feasible only in tunnels with overburdens lower than 100 m. The yield pressure of the support system applied in the squeezing section of the Sedrun Lot of the Gotthard Base Tunnel was equal to about $0.01p_0$. For such realistic p_y/p_0-ratios, the normalized convergence $\varepsilon_{t,c}$ is approximately equal to the axial strain at the centre of the face $\varepsilon_y(0)$ (remember that, according to the last section, unsupported tunnels exhibit $\varepsilon_{t,c}/\varepsilon_y$-ratios between 1 and 2).

4.4 The Effect of a Stiff Support

The stiff support is modelled as an elastic radial support with stiffness k. The radial stiffness k of the ring-shaped lining is equal to $E_L b/a^2$, where a, b, and E_L denote its radius, thickness, and Young's modulus, respectively. The longitudinal bending stiffness of the lining will not be taken into account. The resistance of the lining with the stiffness k is regarded as a boundary condition of the model by imposing a radial pressure $p(y)$ which is proportional to the displacement of the lining at location y and depends,
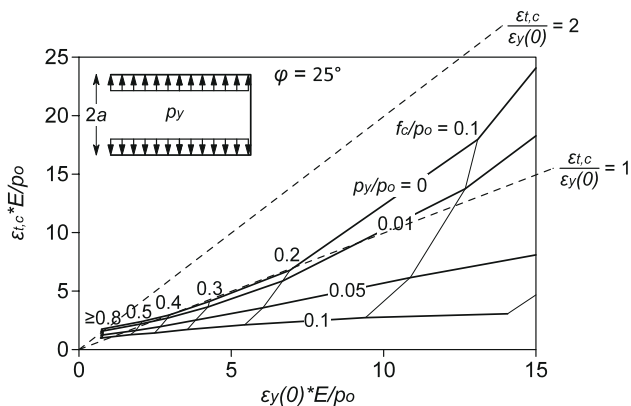
Fig. 12 Tunnel with yielding support. Normalized convergence $\varepsilon_{t,c}E/p_0$ over normalized axial strain at the centre of the face $\varepsilon_y(0)*E/p_0$

therefore, not only on the radial ground displacement $u_r(y)$ but also on its displacement $u_r(e)$ at the installation point $(y = e)$ of the lining (Anagnostou 2007a):

$$p(y) = k(u_r(y) - u_r(e)) \quad (for\ y > e). \tag{13}$$

The parameters k and e have to be considered in addition to the parameters of Eq. 5. The axial strains of the ground at the tunnel axis can thus be expressed as follows (c.f. Eq. 13):

$$\varepsilon_y \frac{E}{p_0} = f_{10}\left(v,\ \varphi,\ \psi,\ \frac{f_c}{p_0}, \frac{y}{a}, \frac{e}{a}, \frac{a\,k}{E}\right) \tag{14}$$

The numerical model is identical to the model of Fig. 7, with the exception of the boundary condition of the tunnel boundary (Eq. 13).

Figure 13a and b shows that the installation of a stiff support close to the face reduces the magnitude of the extrusion, but does not affect the extent of the region ahead of the face influenced by the excavation.

The presence of a lining predictably hinders the development of convergences considerably (Fig. 13c). The closer the lining is installed to the face, the smaller will be the convergences. For linings which are installed very close to the face ($e < a$), the $\varepsilon_{t,c}$ versus ε_y curves are so flat that the extrusion does not provide any useful indication as to the convergence. Figure 13 is computed with a very high stiffness of the lining $k = 1$ GPa/m (e.g. a 0.53 m thick shotcrete lining with a Young's modulus of 30 GPa in a tunnel with diameter of 8 m). The behaviour of soft linings is qualitatively similar to the behaviour of yielding supports (Fig. 12), because both yielding supports and soft linings allow the ground to deform behind the face.

4.5 The Effect of Face Reinforcement

The presence of face reinforcement was considered in a simplified manner by prescribing a uniform pressure p_F on
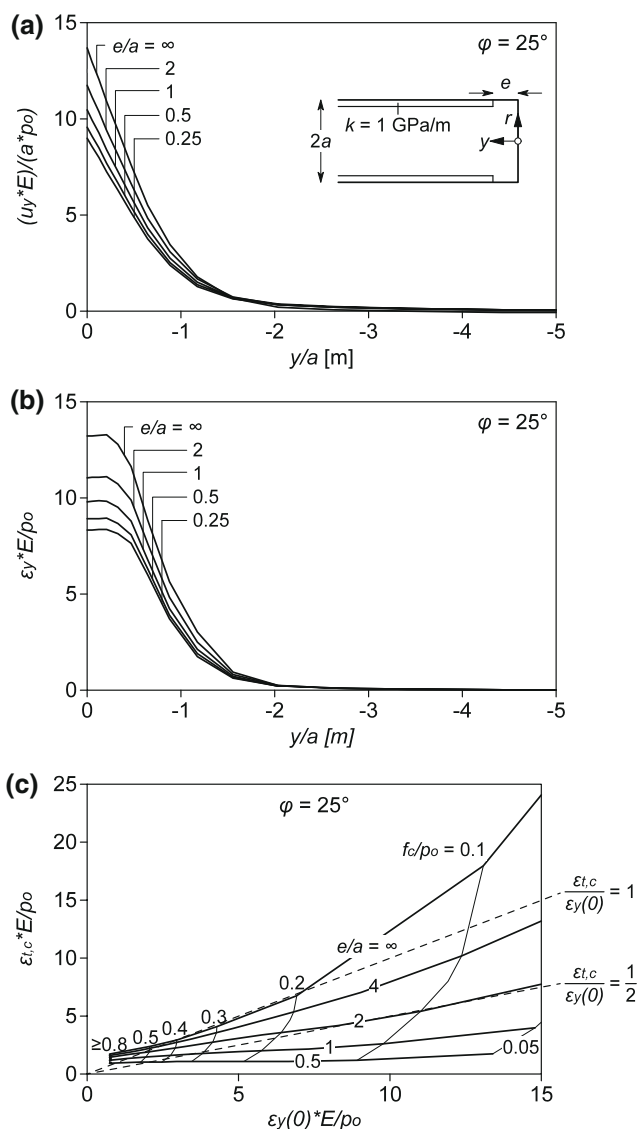

Fig. 13 Tunnel with stiff support. Longitudinal distribution **a** of the normalized axial displacements $u_y*E/(a*p_0)$ and **b** of the strains ε_y*E/p_0; **c** normalized tangential strain $\varepsilon_{t,c}*E/p_0$ over normalized axial strain at the centre of the face $\varepsilon_y(0)*E/p_0$

the face. Peila (1994) and Dias and Kastner (2005) showed that this model is adequate for the determination of the field of displacements ahead of the face. The effect of face support was investigated only for the case of a stiff lining (see Sect. 4.4). As an additional parameter, the normalized face pressure p_F/p_0 must be taken into account in the parameters of Eq. 14:

$$\varepsilon_y \frac{E}{p_0} = f_{11}\left(v,\ \varphi,\ \psi,\ \frac{f_c}{p_0}, \frac{y}{a}, \frac{e}{a}, \frac{a\,k}{E}, \frac{p_F}{p_0}\right). \tag{15}$$

The numerical model is identical to the model of Fig. 7 with the boundary conditions at the tunnel boundary and at the face according to the inset of Fig. 14a. The analysis considers an unsupported length of $e = a/2$.
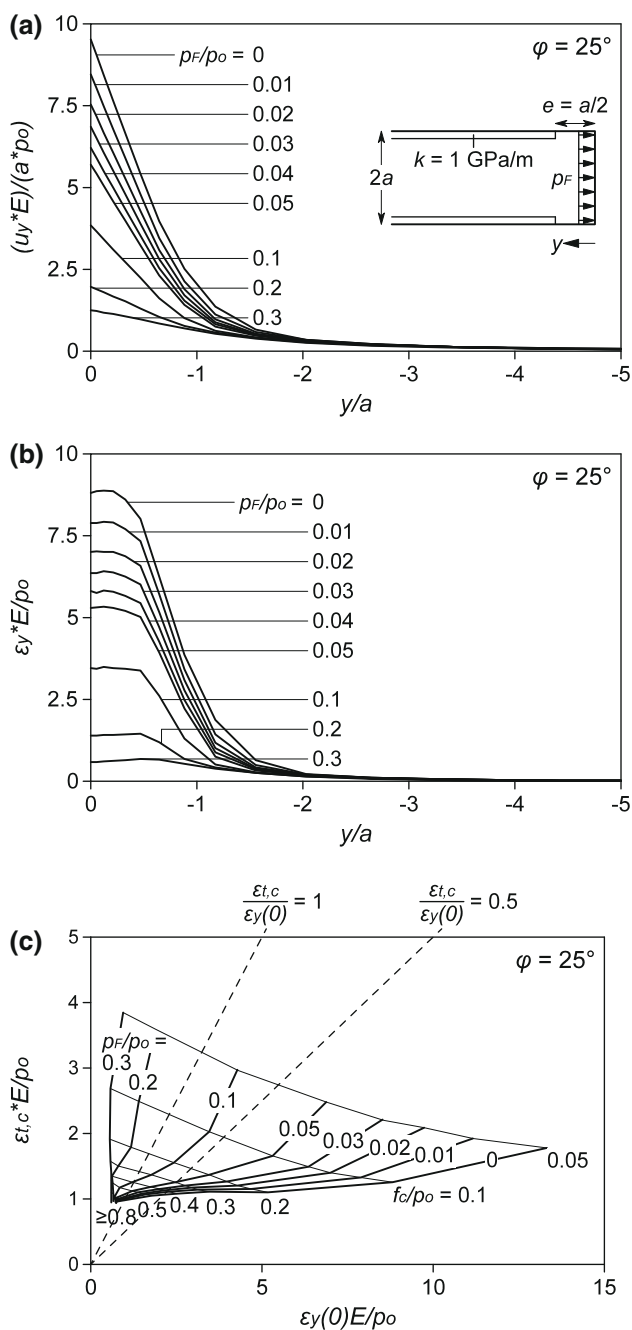
Fig. 14 Tunnel with stiff support and face support. Longitudinal distribution **a** of the normalized axial displacements $u_y*E/(a*p_0)$ and **b** of the strains ε_y*E/p_0; **c** normalized tangential strain $\varepsilon_{t,c}*E/p_0$ over normalized axial strain at the centre of the face $\varepsilon_y(0)*E/p_0$

Figure 14a and b shows that a high support pressure p_F leads to smaller extrusion, but does not affect the influence zone of the advancing face (which extends up to about one diameter ahead of the face). Figure 14c shows that for high face support pressures p_F (>$0.2p_0$), which, however, are feasible only in shallow tunnels, the extrusion of the face does not depend significantly on the ground strength and

cannot be used as an indicator of ground quality. It is remarkable that the higher the face support pressure, the bigger will be the convergences developing over the unsupported span e.

4.6 The Effect of Ground Rheology

4.6.1 Computational Model

Squeezing ground often exhibits a pronouncedly time-dependent response to tunnelling. The deformations in a cavity may continue for several weeks or even months after excavation. As the time scales for core extrusion (a short-term phenomenon) are different to those for convergence (a long-term phenomenon), it is interesting to investigate the extent to which the rheological behaviour of the ground might influence the correlations between these two manifestations of squeezing behaviour.

This issue will be analysed here with the aid of transient stress analyses based on an axisymmetric model of an unsupported tunnel (Fig. 15a). The tunnel advance is simulated with 60 excavation steps, each containing an instantaneous advance of $s = 1$ m, followed by a transient calculation that simulates a standstill period of 1 day. The overall advance rate is, therefore, $v = 1$ m/day. For the purpose of comparisons, the time-independent problem (zero viscosity) was also solved by the step-by-step method. The results are slightly different from those presented in Sect. 4.2.2, where the same problem was solved using the steady state method, which by definition assumes a continuous excavation, i.e. a round length s of zero (Cantieni and Anagnostou 2009a).

The time-dependency of the ground behaviour is handled by means of the elasto-viscoplastic creep model after Madejski (1960), which introduces only one additional parameter to the parameters used in the preceding elasto-plastic computations. The micro-mechanical model consists of an elastic spring in series with a Bingham model (inset of Fig. 15a). The strain rate $\dot{\varepsilon}_{ij}$ is resolved into an elastic and an inelastic part:

$$\dot{\varepsilon}_{ij} = \dot{\varepsilon}_{ij}^e + \dot{\varepsilon}_{ij}^p . \tag{16}$$

The elastic part depends, according to Hooke's law, linearly on the stress rate, while the inelastic part $\dot{\varepsilon}_{ij}^p$, which represents combined viscous and plastic effects, reads according to the classic formulation of Perzyna (1966) as follows:

$$\frac{d\varepsilon_{ij}^p}{dt} = \frac{f}{\eta} \frac{\partial g}{\partial \sigma_{ij}}, \tag{17}$$

where f, g and η denote the yield function, the plastic potential and the viscosity, respectively.

calculation steps:

calculation for excavation n in $\Delta t = 0$
transient calculation with $\Delta t = 1$ day
calculation for excavation (n+1) in $\Delta t = 0$
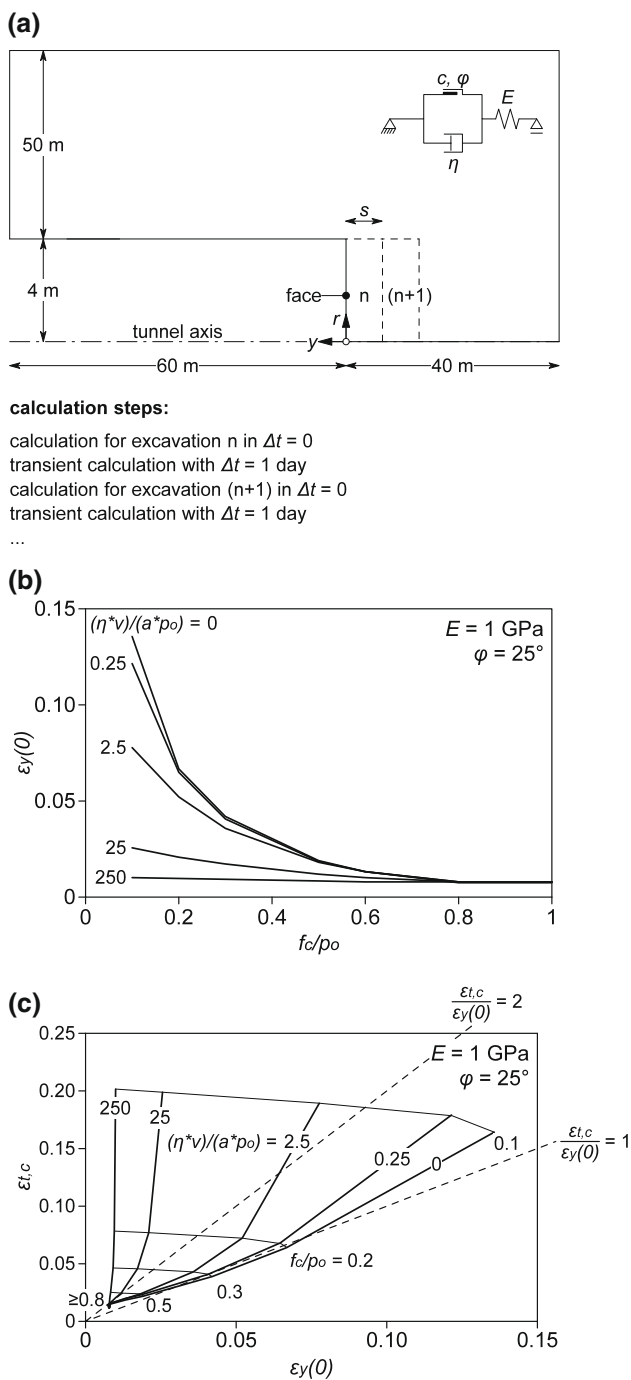transient calculation with $\Delta t = 1$ day
...

Fig. 15 a Problem layout, boundary conditions of the step-by-step numerical model and sequence of the calculation steps (*inset* micromechanical material model); **b** axial strains at the centre of the face $\varepsilon_y(0)$ as a function of the normalized uniaxial strength f_c/p_0; **c** tangential strain at the tunnel boundary $\varepsilon_{t,c}$ as a function of the axial strain at the centre of the face $\varepsilon_y(0)$, the normalized viscosity $\eta^*v/(a^*p_0)$ and the normalized uniaxial compressive strength f_c/σ_0

The calculations have been carried out for different values of the viscosity η. Table 2 shows the other model parameters.

Due to the time dependency of the material behaviour, the displacements of the problem under consideration (Fig. 15a) depend in general on the following parameters:

$$u = f_{12}(E, \ v, \ f_c, \ \varphi, \ \psi, \ \eta, \ p_0, \ a, \ s, t) \tag{18}$$

where s denotes the round length and t the time taken by each excavation round. Considering the gross advance v ($= s/t$) as an independent parameter instead of the round duration t and a dimensional analysis provide the following general expression for the convergence u_c and for the axial strain ε_y at the face:

$$\frac{u_c}{a} = f_{13}\left(v, \ \varphi, \ \psi, \ \frac{E}{p_0}, \frac{f_c}{p_0}, \frac{s}{a}, \ \frac{\eta \, v}{a \, p_0} \right), \tag{19}$$

$$\varepsilon_y = f_{14}\left(v, \ \varphi, \ \psi, \frac{E}{p_0}, \ \frac{f_c}{p_0}, \frac{s}{a}, \ \frac{\eta \, v}{a \, p_0} \right). \tag{20}$$

According to these equations, the response of the model depends on the product of the advance rate v and the viscosity η (cf. Bernaud 1991). The effect of a high advance rate is equivalent to that of a high viscosity. In the borderline case of an "infinitely" rapid excavation, only elastic deformations will occur ahead of the advancing face.

4.6.2 Numerical Results

Figure 15b shows the axial displacements of the centre of the face $u_y(0)$ immediately after the excavation step as a function of the normalized uniaxial compressive strength f_c/p_0 and of the dimensionless parameter $\eta v/(ap_0)$. The curve for $\eta v/(ap_0) = 0$ applies to time-independent ground behaviour. The extrusion of the core is, particularly for low ground strengths, strongly influenced by the viscosity. Viscosity significantly reduces the axial strain at the face, because the development of plastic strains requires more than the short time that is available during ongoing excavation in the vicinity of the tunnel face.

Figure 15c shows the tangential strains at the tunnel boundary $\varepsilon_{t,c}$ as a function of the axial strains at the face $\varepsilon_y(0)$:

- The viscosity η of the ground influences the convergence only slightly. The higher the viscosity, the greater will be the convergence. This is because the pre-deformation of the ground $u_r(y_F)$ is small when the viscosity is high, while the final total radial displacement of the ground developing far behind the face $u_r(\infty)$ is independent of the viscosity and the advance rate in the case of an unsupported tunnel (Bernaud 1991) and was, therefore, calculated with the time-independent plane strain closed-form solution of Anagnostou and Kovári (1993).

- As a consequence of the viscous behaviour (which is decisive mainly for deformations ahead of the face), the ratios of convergence to axial displacement are in general higher than in the case of time-independent behaviour. The rule established in Sect. 4.2.2 (ratio $\varepsilon_{t,c}/\varepsilon_y = 1$–2) is valid only if the dimensionless parameter $\eta v/(ap_0)$ is lower than about 2.5. In the case of a 400 m deep traffic tunnel ($a = 5$ m, $p_0 = 10$ MPa) and a gross advance rate v of 2 m/day, this condition leads to $\eta < 62,500$ kPa*-day, which is typical for materials that respond within a few weeks (Cantieni and Anagnostou 2011).

- At very high viscosities η and advance rates v, the axial strain at the face does not depend significantly on the uniaxial compressive strength f_c of the ground, because the strains developing ahead of the face are almost entirely elastic. In such cases it is impossible to predict the convergences of the opening on the basis of the observed extrusion. Consider, for instance, the curve $\eta v/(ap_0) = 250$. The convergence $u_c = \varepsilon_{t,c} a$ varies between $0.05a$ and $0.20a$ for one and the same axial strain of about 0.01. Also the viscosity η itself represents a source of uncertainty. For an axial strain of 0.025, e.g., the convergence may vary with a factor of about 7 for viscosities between $\eta v/(ap_0) = 2.5$ and 25. Such inaccurate predictions are useless from the practical point of view.

In conclusion, on the one hand, if the ground behaviour is time-dependent, the fact that the core extrusion is low does not necessarily mean that convergences will be small. On the other hand, the large core extrusions are always associated with poor quality ground. It can also be said that a large extrusion represents a sufficient, but not a necessary, condition for large convergences to occur.

4.7 Entering into a Fault Zone

4.7.1 Numerical Model

The present section investigates numerically the evolution of core extrusion and convergence when tunnel advance approaches and enters into an extended, lower quality fault zone, which strikes perpendicularly to the tunnel axis.

The purpose of the present analysis is to find if it is possible at least in principle to recognize a fault zone before entering into it on the basis of the observed extrusion, and if the magnitude of the extrusions provides a useful indication as to the magnitude of the later convergences. Similar numerical analyses have been carried out by Jeon et al. (2005), but these were investigating another question (the possibility of early fault identification on the basis of observed changes in the orientation of the displacement vectors).

The considered axisymmetric numerical model (Fig. 16a) includes a transition zone between the competent rock and the fault zone, where the deformability and strength parameters decrease gradually (Fig. 16b). The excavation was simulated step by step. The 200 m long tunnel was excavated in 100 steps, every excavation step having a length of $s = 2$ m. The calculations have been carried out using the parameters of Table 2 and the deformability and strength parameters of Fig. 16b.

4.7.2 Results

Figure 17a shows the distribution of the axial strain ε_y along the tunnel axis for different positions y_F of the advancing face. The axial strain ahead of the face is similar for all of the excavation steps up to a point that is 4 m ahead of the first change in ground properties at $y = 0$. The shape of the next curve ($y_F = -2$ m) deviates from the preceding one. The strain 2–3 m ahead of the face is significantly higher than for preceding excavation steps. The axial strain ahead of the face increases continuously during the subsequent excavation steps.

Figure 17b shows the influence lines of the average axial strain $\varepsilon_{y,AB}$ for some selected intervals with a length of 0.5 m (every curve in Fig. 17b applies to another interval AB, see inset of Fig. 17b). The intervals starting before $y_A = -2$ m exhibit the same increase in strain for the approaching face. The influence zone of the excavation extends up to about 4 m ahead of the face. The interval starting at $y_A = 0$ (i.e. at the beginning of the transition zone) shows a more pronounced increase of the strains, starting when the advancing face comes to within about 4 m of the interval. The proximate intervals all show a more pronounced increase in the strains again due to the approaching face. After passing the transition zone, the influence lines tend to show the same characteristics. The influence zone of the face increases from initially 4 to 8 m.

Figure 17c shows the radial displacements u_c of selected "measuring" points on the tunnel boundary as a function of their distance from the face. The convergence increases with the advancing face. The maximum convergence increases continuously for the measuring points in the transition zone and in the first 50 m of the fault zone. The increase in the maximum convergences despite the uniform ground conditions prevailing within the fault zone is due to the so-called "wall-effect". The wall-effect describes the stabilizing effect of competent ground on weak ground. The interface shear stresses between the competent and the weak ground reduce the deformations of the weak zone. The wall-effect was analysed by Kovári and Anagnostou (1995) for the borderline case of rigid competent rock and by Cantieni and Anagnostou (2007) for the case of competent rock having a elasto-plastic ground behaviour.
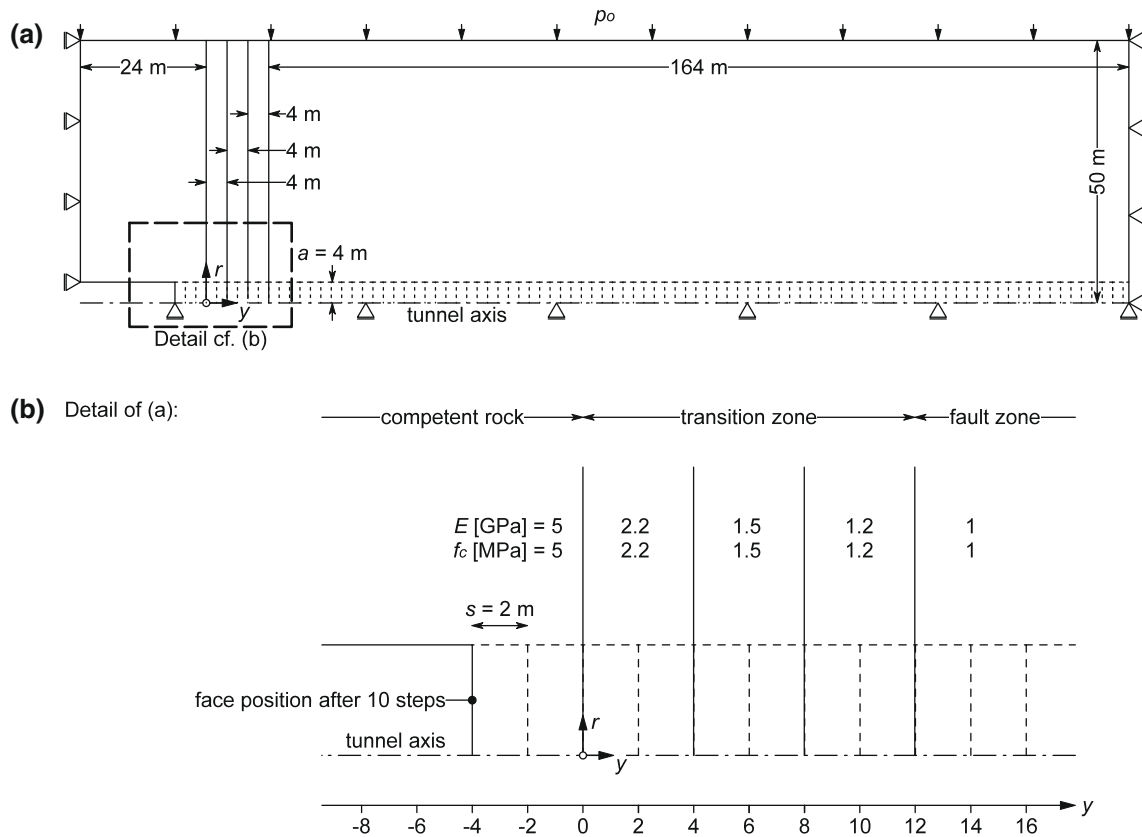
Fig. 16 Fault zone. **a** Axisymmetric numerical step-by-step model and boundary conditions; **b** detail of the transition zone with a gradual decrease in the deformability and strength parameters, including the definition of the chainage y and of the strain intervals AB

The influence lines of the extrusions and the convergences (Figs. 17b and 17c) correlate with each other. Cross sections exhibiting large extrusions also experience high convergences after excavation. A fault zone can thus be detected by monitoring the extrusion of the core ahead of the face (unless the ground exhibits a markedly time-dependent behaviour, see last section).

In a last step, we investigate whether it is possible to predict the convergences (including all spatial effects associated with the fault zone) on the basis of the monitored extrusions, by applying the simple rule established in Sect. 4.2.2. (Section 4.2.2 showed for the case of homogeneous ground, that the ratio of the convergence $\varepsilon_{t,c}$ to the axial strain at the centre of the face $\varepsilon_y(0)$ is in most cases between 1 and 2.) Figure 18a compares the convergences u_c obtained by the numerical computation with the convergences which have been estimated on the basis of the extrusions assuming a ratio $\varepsilon_{t,c}/\varepsilon_y(0)$ of 1, 1.5 or 2. The diagram shows that the assumption of $\varepsilon_{t,c}/\varepsilon_y(0) = 1.5$ leads to convergences which agree very well with the actual convergences. Figure 18b, where the tangential strains $\varepsilon_{t,c}$ are plotted against the axial strains at the face $\varepsilon_y(0)$, shows that most of the points are grouped in the vicinity of the line $\varepsilon_{t,c}/\varepsilon_y(0) = 1.5$.

5 Gotthard Base Tunnel

5.1 Introduction

The present case history investigates the data monitored during construction of the western tunnel of the new Gotthard Base Tunnel, which crosses the northern intermediate Tavetsch formation (the so-called TZM formation) and the adjacent Clavaniev zone (referred to as "CZ" in Fig. 19).

The aim of the present case history is to find out whether there is a correlation between the extrusion of the core and the convergences of the tunnel and, accordingly, if it would have been possible to predict the convergences solely on the basis of the monitored extrusions. The present case history will focus on two reaches, where the extrusion of the core has been monitored with a series of so-called reverse-head-extensometers (RH-extensometers; Thut et al. 2006). The first reach reaches from chainage 1,690 m to chainage 1,780 m of the western tube excavated northwards (NW tube). The second reach starts at chainage 1,980 m and ends at chainage 2,140 m of the NW tube (Fig. 19b).
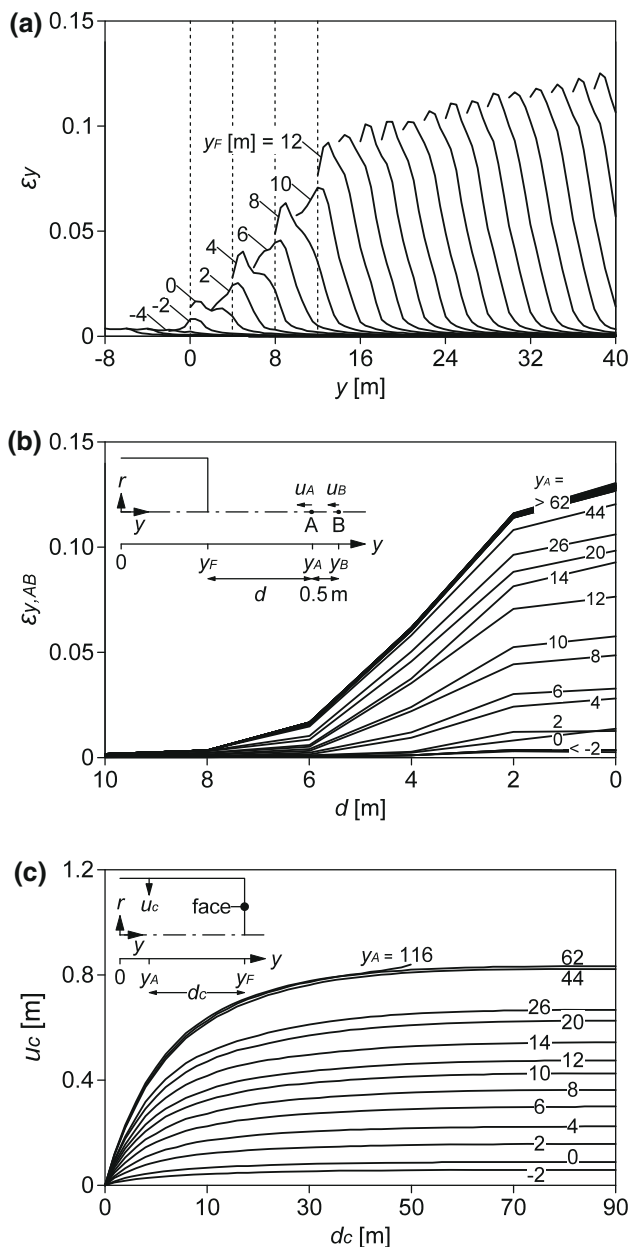
Fig. 17 a Axial strain ε_y profiles for all face positions between $y = -8$ and 38 m; **b** influence lines of the axial strain ε_y; **c** influence lines of the radial displacements u_c of selected points on the tunnel boundary
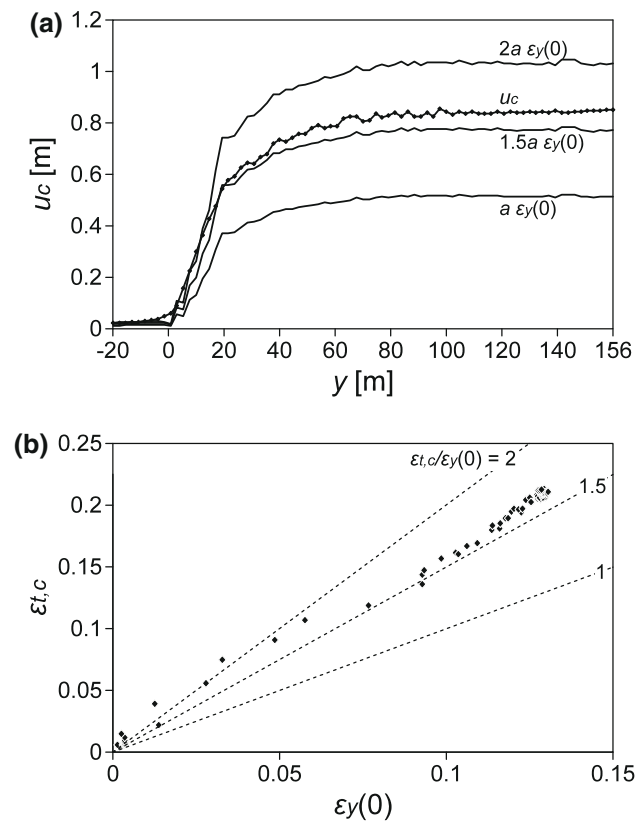

Fig. 18 a Comparison of the ground convergences u_c (= $\varepsilon_{t,c}*a$) at chainage y with the convergences calculated on the basis of the face extrusions $\varepsilon_y(0)$ with the ratios $\varepsilon_{t,c}/\varepsilon_y(0)$ of 1, 1.5 and 2; **b** tangential strain $\varepsilon_{t,c}$ over axial strain at the centre of the face $\varepsilon_y(0)$ for all chainages y in the fault zone model

5.2 Geological and Geotechnical Properties

The tunnel crosses the northern TZM formation and the Clavaniev zone for about 1,150 m at a depth of 800 m (Fig. 19b). The Clavaniev zone denotes the tectonically intensively sheared southern part of the Aar-massif between the Aar-massif and the TZM formation (cf. Schneider 1997). The Clavaniev zone was encountered over about 120 m at the end of the advance before entering into the competent rocks of the Aar-massif (Fig. 20b). Both, the TZM formation and the Clavaniev zone are characterized by alternating layers (which have a thickness in the range of decimetres to decametres) of intact and more or less kakiritic gneisses, slates, and phyllites (Fig. 20c). The term "kakirite" denotes a broken or intensively sheared rock, which has lost a large part of its original strength (cf. Schneider 1997; Vogelhuber 2007). The orientation of the layers to the tunnel axis varies from perpendicular to parallel (Fig. 20d).

On account of the expected squeezing conditions, the geological survey included an inclined, exploratory borehole SB 3.2, which was over 1,700 m deep and which passed through the problematic series of rocks (Fig. 19b). The core samples retrieved from the boring were used to carry out a laboratory testing programme to investigate the strength and deformation properties of the weakest zones. The testing program was carried out at the Institute for Geotechnical Engineering of the ETH Zurich (Vogelhuber 2007), and also continued during construction of the tunnels with rock samples retrieved by horizontal drillings performed from the tunnel face (Anagnostou et al. 2008).
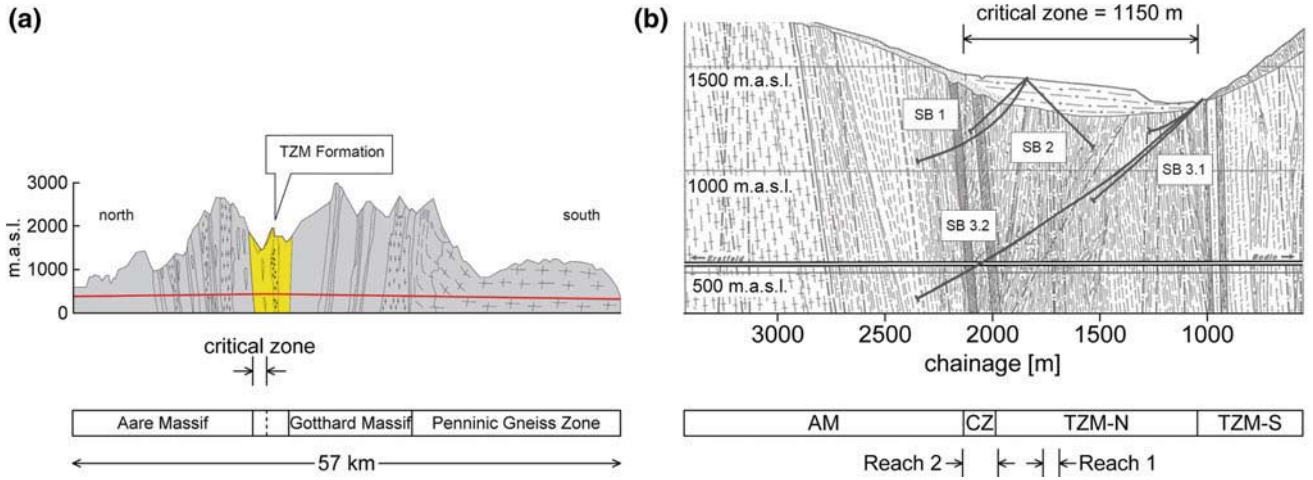
Fig. 19 a Gotthard Base Tunnel: schematic representation of the longitudinal geological section with the squeezing TZM formation (after Kovári 2009); **b** detail of the TZM formation (after Vogelhuber 2007) showing the Aare massif (*AM*), the Clavaniev zone (*CZ*), the northern TZM formation (*TZM-N*), the southern TZM formation (*TZM-S*) and the two reaches under consideration
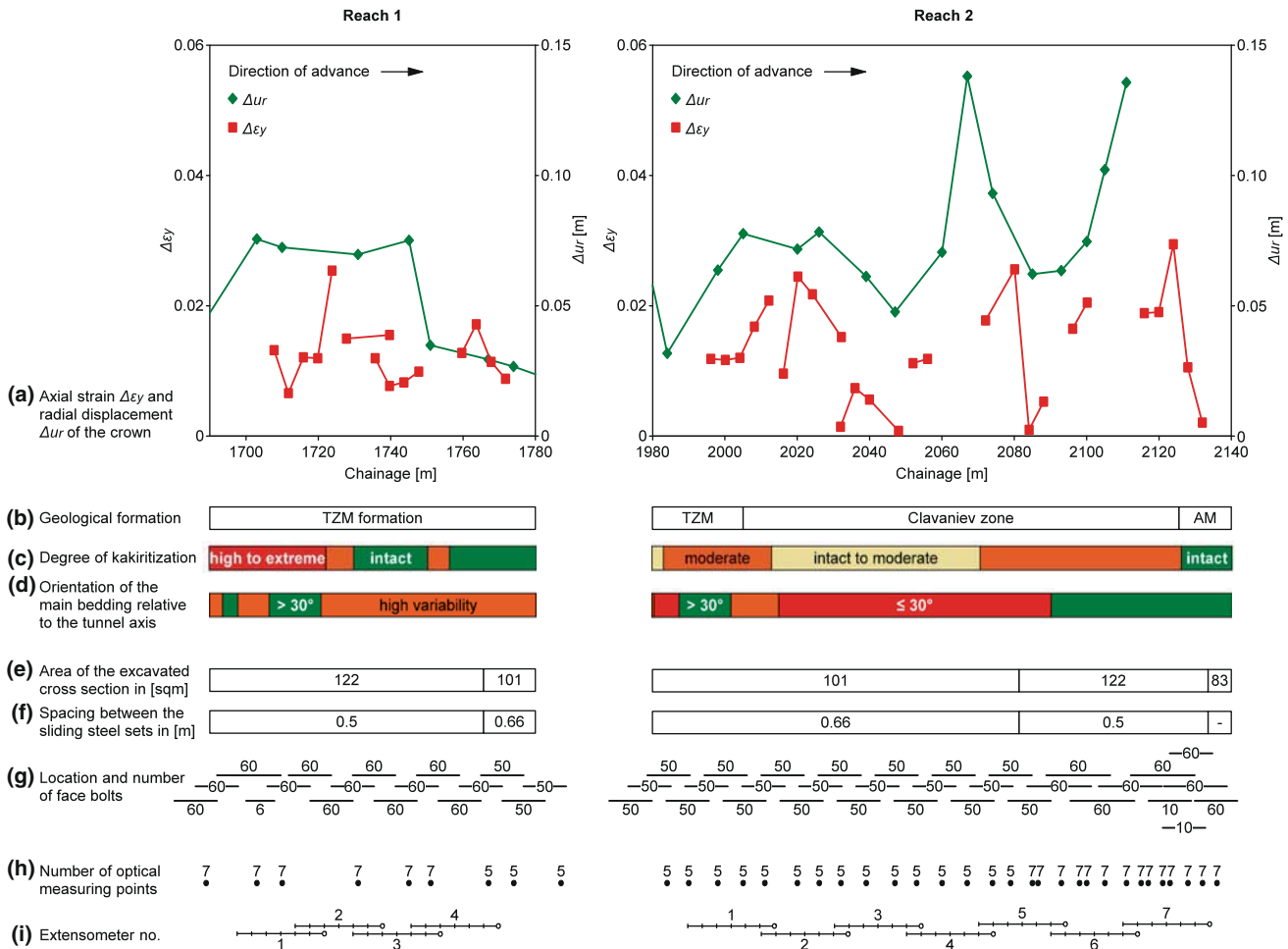

Fig. 20 Axial strain $\Delta\varepsilon_y$ and radial displacement Δu_r of the crown plotted along the alignment of reach 1 and 2 (**a**), including information about the actual geology (**b–d**), the support measures applied (**e–g**) and the monitoring setup (**h, i**)

Most of the samples were tested by means of so-called multistage triaxial tests under consolidated and drained conditions (CD-tests). Prior to the consolidation and shearing phases, the testing procedure included a watering phase to saturate the sample and to determine the permeability of the material (Vogelhuber 2007).

Figure 21 shows a sample of a kakiritic rock before and after a triaxial test, while Fig. 22 summarizes the strength properties of kakiritic rock samples obtained during tunnel construction. The deformability properties have also be determined with triaxial testing. The test results showed that the Young's modulus increases with increasing confining stress. The Young's moduli obtained by Vogelhuber (2007) ranged from about 0.5 GPa to 6 GPa for effective confining stresses of 1–9 MPa.

The water table was detected to be close to the ground surface, namely 800 m above the tunnel. Most of the kakiritic rocks had a permeability between 2×10^{-10} and 2×10^{-9} m/s.

5.3 Construction Method

The tunnel was excavated full-face. Squeezing was tackled through a yielding support system consisting of two rings of sliding steel sets (TH 44/70) lying one upon the other and connected by friction loops (Ehrbar and Pfenninger 1999; Kovári et al. 2006; Kovári and Ehrbar 2008). Figure 23 shows the longitudinal and the cross section of the yielding support system. In the tunnel reaches under investigation, the radial over-excavation (which is required for accommodating the deformations) was either 0.5 or 0.7 m, the cross section area $A_F = 101$ or 122 m^2, respectively, and the spacings of the steel sets 0.66 or 0.5 m, respectively. Up to 190 m radial bolts with a length of 8 m were installed over the whole circumference per meter of tunnel. The face was supported by about 50 to 60 bolts with a length of 12–18 m, and with an overlap of about 6 m. After the rate of convergence slowed down, a shotcrete ring of 0.5 m was applied (normally at a distance of about 30 m behind the face). The area of the excavated cross section and the support measures applied are summarized in Fig. 20e to 20g.

5.4 Monitoring

The convergences of the opening were monitored optically with 5 or 7 points per cross section. The distance between the monitored cross sections was between 5 and 20 m. The

Fig. 21 Rock sample with an extreme degree of kakiritization retrieved during construction from the TZM formation before (*left*) and after (*right*) the triaxial test

Fig. 22 **a** Measured effective cohesion c' over measured effective angle of internal friction φ'; **b** distribution of the effective cohesion c'; **c** distribution of the angle of internal friction φ' of the kakiritic samples tested during the construction of the Gotthard Base Tunnel (only samples which failed isotropically are considered) (after Anagnostou et al. 2008)
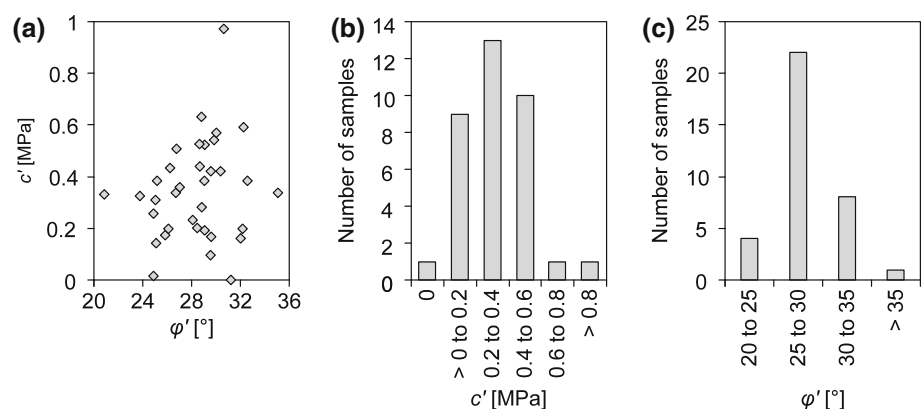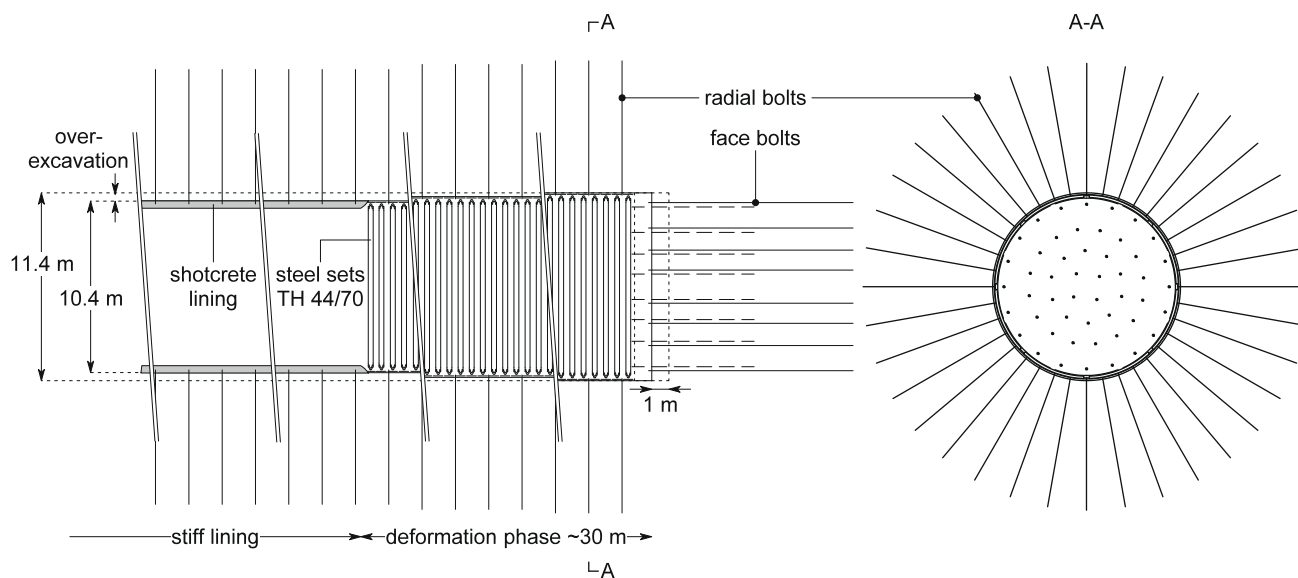
Fig. 23 Longitudinal section and cross section of the yielding support system realized in the northern TZM formation (after Ehrbar and Pfenninger 1999)

exact location and number of monitored points per cross section along the tunnel alignment are shown in Fig. 20h.

The core extrusion was monitored by 4 RH-extensometers in the first reach (TZM formation) and 7 RH-extensometers in the second reach (Clavaniev zone). The RH-extensometers were placed at the axis of the tunnel. They had a length of 24 m and overlapped 4–8 m with the preceding ones. The position of the measuring head and the six measuring points of each extensometer with respect to the tunnel alignment are shown in Fig. 20i.

5.5 Data Analysis

5.5.1 Primary Data

Figure 24a and b shows the primary data obtained by the RH-extensometers of reaches 1 and 2, respectively. The wavelike shape of the curves which show the extrusion over time, indicates that the ground exhibits a time-dependent behaviour. Every excavation step accelerates the development of the extrusions before they slow down until the next excavation step again accelerates the rate of deformations. The extrusions monitored consist of an instantaneous part, which is caused by the stress redistribution produced by each excavation step, and a time-dependent part produced by rock creep and consolidation processes. After an excavation step, the extrusions continue for several days. For instance, the last measuring point of extensometer 5 at chainage 2,090 m of reach 2 shows the extrusion that developed at a distance of 4 m ahead of the face during a standstill of 30 days (curve B in Fig. 24b).

The extrusion rate is almost zero after 30 days and accelerates when the excavation is restarted. The measurements indicate that 95% of the final extrusion is reached after about 20 days. This indicates a viscosity η of about 10^4 to 10^5 kPa*day (cf. Cantieni and Anagnostou 2011).

To assess the behaviour of the ground along the tunnel it is necessary to compare deformations that occur under similar conditions and, more specifically, during the same period of time. As the duration of the advance halts varied between the different stretches of the tunnel, the comparability of the final extrusion values would be questionable. Therefore, the present analysis considers only the extrusions developing during the excavation round and the 10 h following excavation. Figure 24c shows by means of an example the way the extrusions have been determined.

5.5.2 Influence Lines

Due to the low spatial resolution of the monitored profile (the relatively small number of measuring points) and to the large number of readings, the most meaningful way to present the monitoring data is to plot influence lines.

Figures 25 and 26 show the influence lines of the axial strain ε_y (taking account of the extrusion generated by face advances and during the 10 h following each advance) for all extensometers. The characteristics of the influence lines are similar for all extensometers. The observation that the strains increase continuously until $d = 0$, contradicts with the theoretical predictions, according to which the strain should not increase close to the advancing face (Fig. 9b). The reason for the different behaviour is the length of the
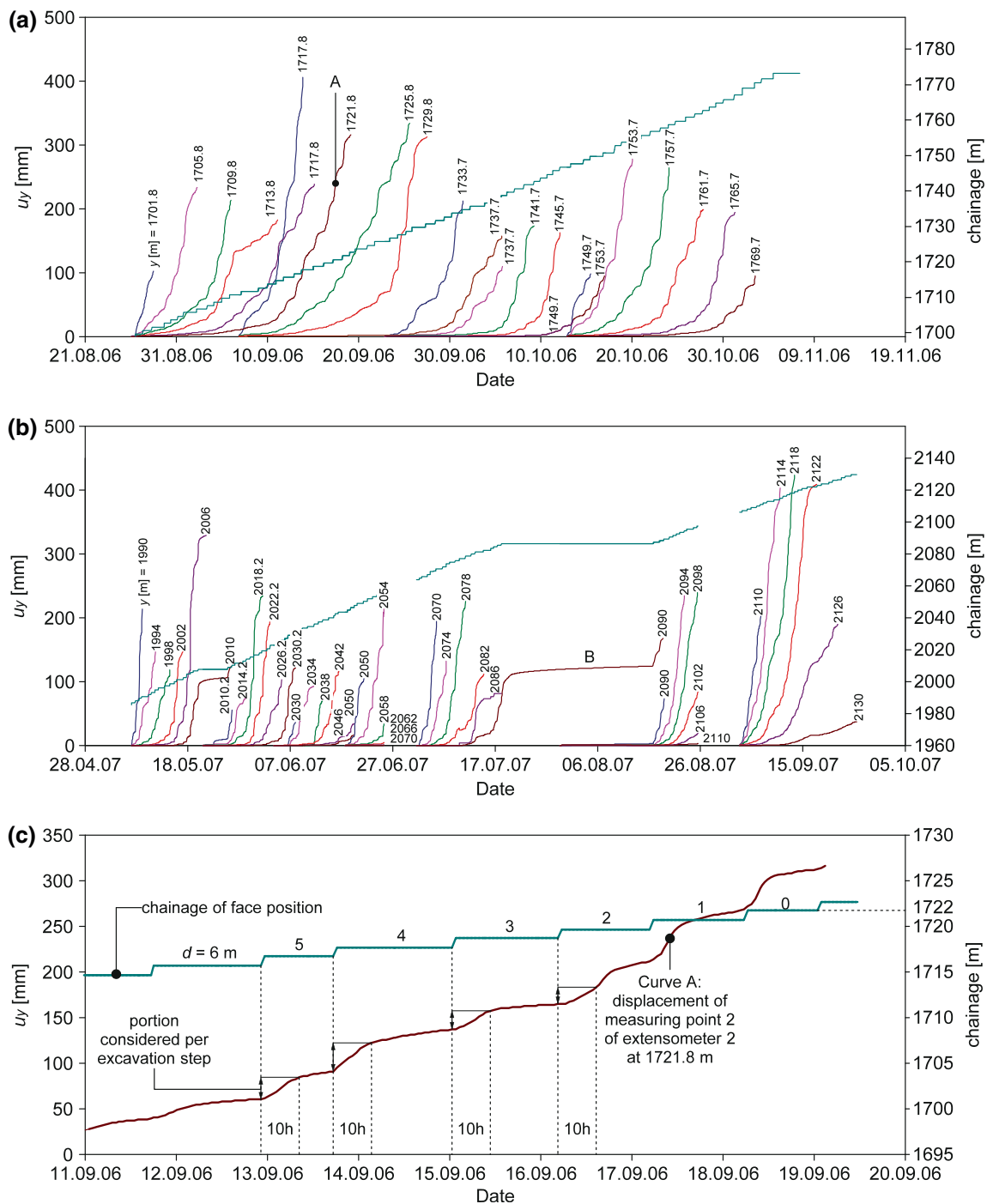
Fig. 24 **a** Extrusions u_y over time for the measuring points of reach 1 (**a**) and of reach 2 (**b**) of the NW tube; **c** illustration of the determination of extrusions from the example of curve A of Fig. 24a

interval (4 m). The average strain over a 4 m long interval increases until the face reaches the interval ($d = 0$), even if the strain locally close to the face remained constant over the last meters.

Variations in the magnitude of the strain, as well as in the extent of the influence zone of the advancing face, indicate changes in the quality of the core ahead of the

face (the support measures are assumed to be constant). Figure 25 shows the influence lines of the axial strain ε_y over tunnel reach 1. The last interval of extensometer 3 shows an increase (at about 11 m) in the strain earlier than the other intervals (at about 7 m) of the same extensometer. The influence lines of extensometer 4 confirm this trend.
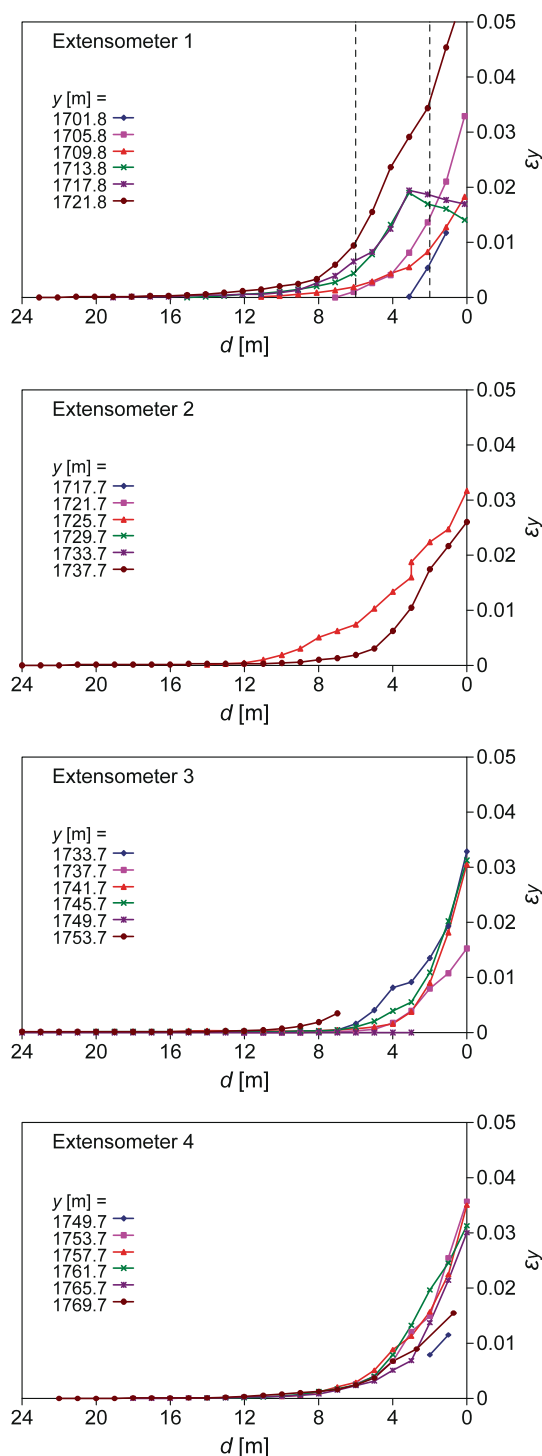
Fig. 25 Influence lines of axial strain ε_y for the intervals between the measuring points at chainage y and $(y + 4\ m)$ of extensometer 1–4 of reach 1

Consider now the *maximum* strain, i.e. the strain developing up to the time point where the face reaches the first measuring point ($d = 0$). It is possible to distinguish three cases: Most of the measurements show maximum

strains of 0.03. Exceptions with lower maximum strains are the interval 1,709.8 m of extensometer 1, 1,737.7 m of extensometer 3 and 1,769.7 m of extensometer 4. The interval 1,721.8 m of extensometer 1 shows a considerably higher maximum strain than all other intervals. The intervals 1,713.8 and 1,717.8 m also tend to such high values. But at $d = 3$ m, the strain suddenly decreases with the approaching face. A decrease in strain indicates an axial re-compression of the rock over the considered interval. This behaviour cannot be traced back to the effect of a heavier face support, because this effect is very small at the actual initial stress level (see curve $0.01p_0$ in Fig. 14b). Besides measuring errors, this behaviour could be due to the presence of a very strong ground interlayer perpendicular to the tunnel axis, which hinders the axial deformation and thus recompresses the weak ground further away from the face.

Figure 26 shows the influence lines of the axial strain ε_y over tunnel reach 2. Extensometer 6 clearly shows that the influence zone of the considered intervals increases continuously. This observation provides an indication of decreasing ground quality (as shown later, the convergences also increase in this portion). Extensometers 3 and 4 appear to be in a more competent rock than the others. The influence zone of the face is considerably less extended (about 6 m) than in most of the other intervals of tunnel reach 2 (between 8 and 12 m) and the extrusion values are also lower (2%). In the next section, we will see that also the convergences are lower in this tunnel portion.

5.5.3 Extrusions Versus Convergences

The next step is to compare the longitudinal distribution of the extrusion with the distribution of the convergences. To obtain comparable values, the analysis considers as a measure of the extrusion the strain that develops due to the advance of the face from a distance of 6 m to a distance of 2 m in respect of each ground interval (see the strain portion between the vertical dashed lines in the diagram of extensometer 1 in Fig. 25 and the upper part of Fig. 27). The reason for selecting this interval (6–2 m) was to maximize the number of measuring points that could be used for the analysis.

The radial displacement of the tunnel crown is used as a measure of convergence. To get comparable values, the analysis takes into account only a specific portion of the monitored displacements, occurring due to a face advance of 25 m. More specifically, we consider the displacement that develops as the distance from the face to the monitoring section increases from 5 to 30 m (see the lower part of Fig. 27). This interval was chosen because the latest zero reading of a measuring point in the reaches under consideration was made at about 5 m behind the face, and because the shotcrete ring (which practically prevents
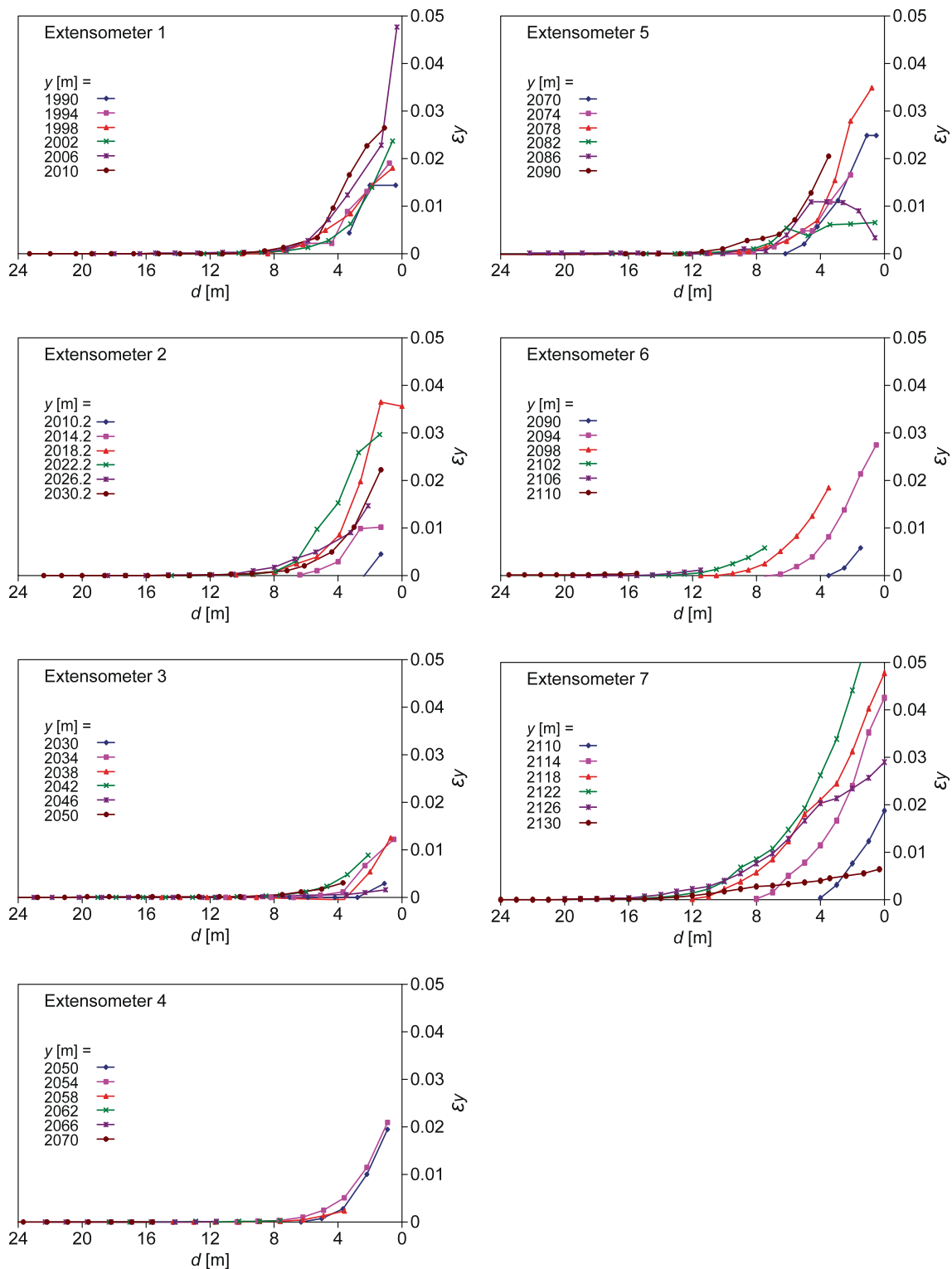
Fig. 26 Influence lines of axial strain ε_y for the intervals between the measuring points at chainage y and $(y + 4 \text{ m})$ of extensometer 1–7 of reach 2

deformations) is applied at a distance of about 30 m from the face. Figure 28 shows the radial displacements Δu_r of the crown for different cross sections as a function of their distance to the face d_c. Most of the curves of Fig. 28 show convergences (in respect of a face advance from 5 to 30 m ahead of the monitored point) of between 0.06 and 0.08 m.
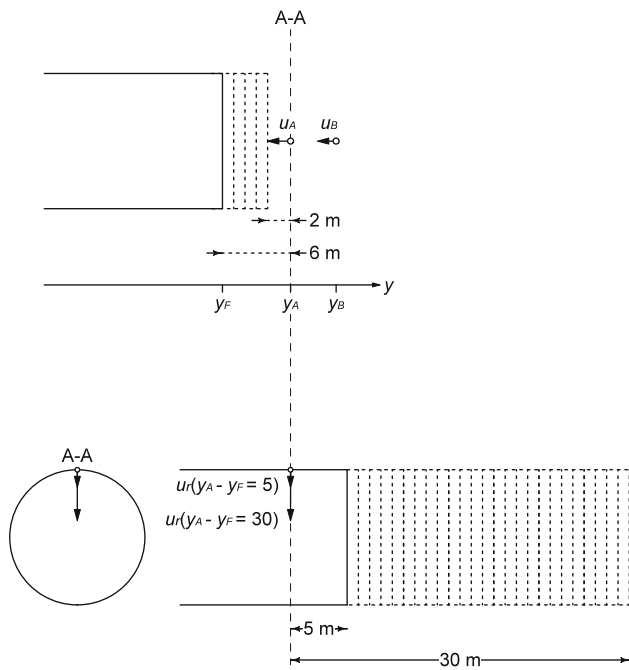
Fig. 27 Method for determining, (i), the accumulated strain $\Delta\varepsilon_y$ ahead of the face for an excavation advance from 6 to 2 m ahead of each measuring point and, (ii), the radial displacements of the crown Δu_r of the tunnel generated due to an excavation advance of 25 m

Figure 20a shows the axial strain and radial displacements of the crown along tunnel reaches 1 and 2. The figure includes only the measuring points which worked properly during the monitored face advance. (Some measuring points failed because the bar which connects the measuring point with the measuring head, was damaged by face bolt drillings.) The convergences in tunnel reach 2 exhibit a weak correlation with the extrusions. The decrease in convergences before reaching chainage 2,050 m, and the subsequent increase in convergences were indicated by a decrease and an increase in extrusions. The change in convergences appeared even without a significant change in the geology, construction method or overburden. Also, the decrease and increase in convergences around chainage 2,090 m are indicated by a decrease and a subsequent increase in extrusions.

No correlation can be observed between the convergences and the extrusions in tunnel reach 1. The decrease in convergences after chainage 1,745 m could not be predicted on the basis of the observed extrusions. One reason for the lack of correlation may be the arrangement of the monitoring stations. In alternating layers of weak and hard rock the variation in convergences can be significant even over short distances and can thus not be monitored completely if the distance between the monitoring stations is large (Cantieni and Anagnostou 2007).
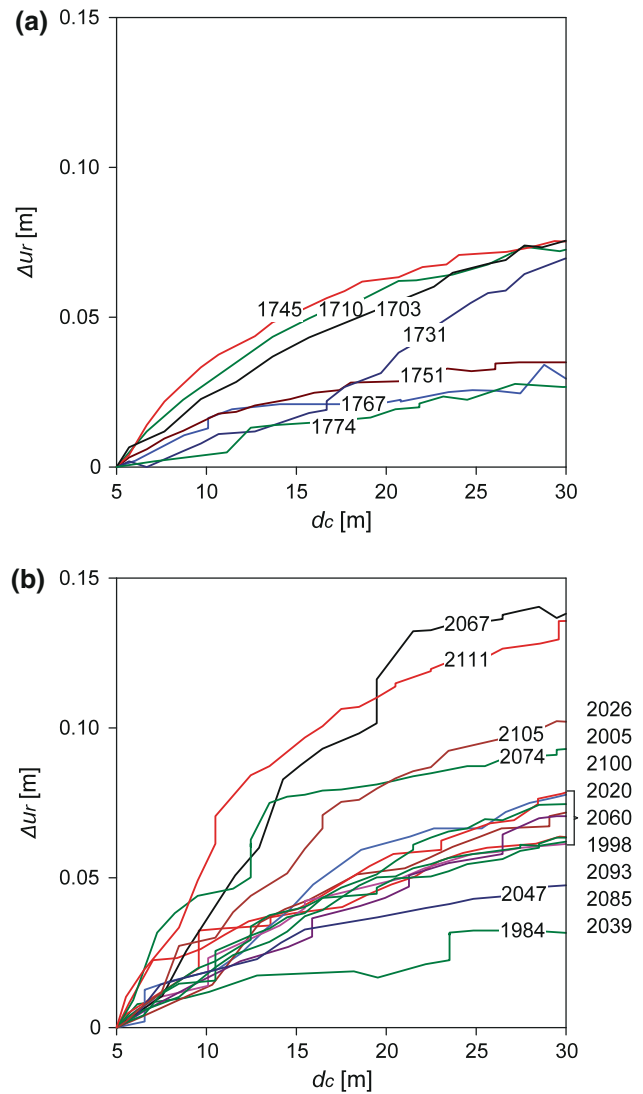

Fig. 28 **a** Convergences as a function of the distance to the face d_c; **a** for reach 1 and **b** for reach 2

Figure 29 shows the normalized displacement of the tunnel crown ($\Delta\varepsilon_{t,c} = \Delta u_r/a$) as a function of the axial strain $\Delta\varepsilon_y$ of the core for the two tunnel reaches. The points from tunnel reach 2 are roughly grouped around a slightly inclined straight line. Note that the deformations plotted in Fig. 29 are not the total deformations, but only the deformations that developed due to the specific face advances mentioned above. For this reason, Fig. 29 cannot be compared directly to the similar diagrams of Sect. 4, which consider the total deformations. A qualitative comparison is nevertheless possible. The relationship between the extrusions and the convergences is similar to the relationship between the numerical results for a yielding support shown in Fig. 12 and for the stiff support shown in Fig. 13, where the convergences do not vary significantly compared to the extrusions. This behaviour seems reasonable because
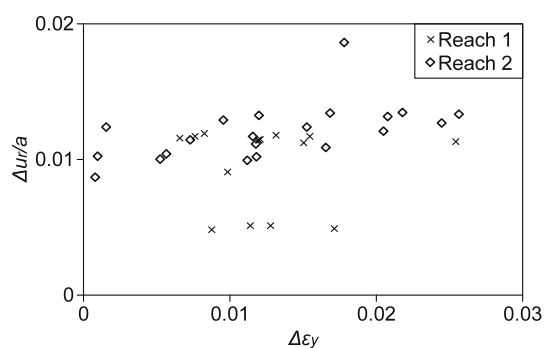
Fig. 29 Normalized displacement of the tunnel crown $\Delta u_r/a$ at the tunnel crown as a function of the axial strain $\Delta \varepsilon_y$ for reaches 1 and 2

the support system applied is a yielding support, which is set rigidly at a distance of about 30 m ($e/a = 5$) behind the face. Furthermore, the big variation in the extrusions indicates that the effect of the time-dependency of the ground and of the face support is of subordinate importance in the present case history (cf. Figures 14 and 15). For a ground viscosity η between 10^4 and 10^5 kPa*day, an advance rate of $v = 1$ m/day and an initial stress of $p_0 = 20$ MPa the normalized viscosity $\eta v/(ap_0)$ is between 0.08 and 0.8. According to Fig. 15, such viscosities influence the extrusions only slightly.

6 Conclusions

The extrusion of the core is affected by ground quality, the initial stress state and the construction method. Stiff supports which are installed close to the face reduce the magnitude of the extrusions, as do yielding supports (although to a lesser extent). Face reinforcement also reduces the magnitude of extrusions. However, the effect of yielding supports and face support on extrusion is less pronounced in deep tunnels.

It is theoretically possible to predict ground response by means of extrusion measurements when the ground exhibits only a moderately time-dependent behaviour. The time-independent numerical analysis of tunnelling into a fault zone showed that the convergences can even be estimated in heterogeneous ground. Pronounced time-dependent ground behaviour makes it very difficult to predict the ground response, because extrusions are governed by short-term behaviour, while the final ground response is governed by long-term behaviour. A large extrusion represents a sufficient, but not a necessary, condition for large convergences to occur.

The analysis of the extrusions by means of the axial strains instead of the axial displacements makes it possible to use a longer portion of the measuring device, because the error introduced by a non-fixed reference point can be avoided. As shown by the case history of the Tartaiguille tunnel, it is possible to use an even longer portion of the measuring device if the increase in strains due to the specific face advance is analysed. Such an analysis is also independent of the deformations which the ground experiences before the installation of the measuring device.

The case history of the Raticosa tunnel and the numerical calculations showed that the extrusion does not provide any useful indication as to the convergence in case of stiff linings which are installed close to the face, because in such cases the convergences are small and almost independent of the ground quality.

The case histories of the Vasto tunnel and the Gotthard Base Tunnel show that there is a weak correlation between the axial extrusions and convergences of the tunnel. In the case of the Gotthard Base Tunnel, a correlation might have been especially helpful as the convergences changed even without a significant variation in the geology, construction method or overburden. However, there was no clear correlation that would make it possible to predict convergences with sufficient reliability on the basis of extrusion monitoring alone. The extrusion data should be evaluated in combination with other information, such as advance probing. The main advantage of extrusion monitoring was rather in the early detection of deformations which might lead to face loosening and instability.

References

Anagnostou G (2007a) Continuous tunnel excavation in a poro-elastoplastic medium. In: Pande, Pietruszczak (eds) Numerical models in geomechanics (NUMOG X), Rhodes, Greece, pp 183–188

Anagnostou G (2007b) Practical Consequences of the Time-Dependency of Ground Behavior for Tunneling. In: Traylor MT, Townsend JW (eds) Rapid Excavation and Tunneling Conference, Toronto, pp 255–265

Anagnostou G, Kovári K (1993) Significant parameters in elasto-plastic analysis of underground openings. J Geotech Eng 119(3):401–418

Anagnostou G, Kovári K (2005) Tunnelling through geological fault zones. In: International symposium on design, construction and operation of long tunnels, Taipei, pp 509–520

Anagnostou G, Pimentel E, Cantieni L (2008) Report on behalf of AlpTransit AG: Felsmechanische Laborversuche Los 378—Schlussbericht—AlpTransit Gotthard Basistunnel, Teilabschnitt Sedrun. ETH Zurich, Institute for Geotechnical Engineering. Chair of Underground Construction, Zurich

Barla G (2005) Large size tunnels excavated full face in difficult conditions. In: Löw (ed) Geologie und Geotechnik der Basistunnels am Gotthard und am Lötschberg, Zurich, pp 275-286

Barla G (2009) Oral Communication 7th Mai 2009. Zürich

Barla G, Barla M (2004) Discussion on the full face method. Felsbau 22(4):26–30

Barla G, Barla M, Bonini M (2004) Characterisation of Italian Clay Shales for Tunnel Design. Int J Rock Mech Min Sci 41 (3):CD-ROM—Proceedings of SINOROCK2004 Symposium

Bernaud D (1991) Tunnels profonds dans les milieux viscoplastiques: approches expérimentale et numérique. PhD Thesis, Ecole Nationale des Ponts et Chaussées, Paris, France

Bernaud D, Maghous S, Buhan Pd, Couto E (2009) A numerical approach for design of bolt-supported tunnels regarded as homogenized structures. Tunn Undergr Space Technol 24:533–546

Boldini D, Graziani A, Ribacchi R (2004) Raticosa tunnel, Italy: characterization of tectonized Clay-Shale and analysis of monitoring data and face stability. Soils Found 44(1):57–69

Bonini M (2003) Mechanical behaviour of Clay-Shales (Argille Scagliose) and implications on the design of tunnels. Ph.D. Thesis, Politecnico di Torino, Torino, Italy

Bonini M, Debernardi D, Barla M, Barla G (2009) The mechanical behaviour of Clay Shales and implications on the design of tunnels. Rock Mech Rock Eng 42(2):361–388. doi: 10.1007/s00603-007-0147-6

Cantieni L, Anagnostou G (2007) On the variability of squeezing in tunneling. In: Ribeiro e Sousa L, Olalla C, Grossmann NF (eds) 11th Congress of the International Society for Rock Mechanics, Lisbon, pp 983–986

Cantieni L, Anagnostou G (2009a) The effect of the stress path on squeezing behaviour in tunnelling. Rock Mech Rock Eng 42(2):289–318. doi:10.1007/s00603-008-0018-9

Cantieni L, Anagnostou G (2009b) The interaction between yielding supports and squeezing ground. Tunn Undergr Space Technol 24(3):309–322. doi:10.1016/j.tust.2008.10.001

Cantieni L, Anagnostou G (2011) On a paradox of elasto-plastic tunnel analysis. Rock Mech Rock Eng 44:129–147. doi: 10.1007/s00603-010-0126-1

Cosciotti L, Fazio AL, Boldini D, Graziani A (2001) Simplified behavior models of tunnel faces supported by shotcrete and bolts. In: al Ae (ed) Modern Tunneling Science and Technology, pp 407–412

De Biase A, Grandori R, Bertola P, Scialpi M (2009) Gibe II Tunnel Project—Ethiopia: 40 Bars of Mud Acting on the TBM "Special Designs and Measures Implemented to Face One of the Most Difficult Events in the History of Tunneling". In: Almeraris G, Mariucci B (eds) Rapid Excavation and Tunneling Conference. Las Vegas, Nevada, pp 151–170

Dias D, Kastner R (2005) Modélisation numérique de l'apport du renforcement par boulannage du front de taille des tunnels. Can Geotech J 45:1656–1674. doi:10.1139/T05-086

Eclaircy-Caudron S, Dias D, Kastner R (2009) Displacements and stresses induced by a tunnel excavation: Case of Bois de Peu (France). In: Ng HL (ed) Geotechnical aspects of underground construction in soft ground, Shanghai, China, pp 373–379

Egger P (1980) Deformation at the face of the heading and determination of the cohesion of the rock mass. Undergr Space 4:313–318

Ehrbar H, Pfenninger I (1999) Umsetzung der Geologie in technische Massnahmen im Tavetscher Zwischenmassiv Nord. In: Vorerkundung und Prognose der Basistunnels am Gotthard und am Lötschberg, Symposium Geologie Alptransit, Zurich, Switzerland, pp 381–394

Ghaboussi J, Gioda G (1977) On the Time-Dependent Effects in Advancing Tunnels. Int J Numer Anal Methods Geomech 1:249–269

Hoek E (2001) Big tunnels in bad rock. J Geotech Geoenviron Eng 127(9):726–740

Jeon JS, Martin CD, Chan DH, Kim JS (2005) Predicting ground conditions ahead of the tunnel face by vector orientation analysis. Tunn Undergr Space Technol 20:344–355

Kovári K (1998) Tunnelling in squeezing rock. Tunnel 5:12–31

Kovári K (2009) Design Methods with Yielding Support in Squeezing and Swelling Rocks. In: World Tunnel Congress, Budapest, Hungary

Kovári K, Anagnostou G (1995) The ground response curve in tunnelling through short fault zones. In: Fujii T (ed) 8th Congress of the International Society for Rock Mechanics, Tokyo, pp 611–614

Kovári K, Ehrbar H (2008) Gotthard Basistunnel, Teilabschnitt Sedrun—Die druckhaften Strecken im TZM Nord: Projektierung und Realisierung. In: Swiss Tunnel Congress, Luzern, pp 39–47

Kovári K, Lunardi P (2000) On the Observational method in tunneling. In: GeoEng 2000, Melbourne

Kovári K, Amstad C, Koppel H (1979) New developments in the instrumentation of underground openings. In: Proceedings of the 4th Rapid Excavation and Tunnelling Conference, Atlanta, USA

Kovári K, Ehrbar H, Theiler A (2006) Druckhafte Strecken im TZM Nord: Projekt und bisherige Erfahrungen. In: Löw (ed) Geologie und Geotechnik der Basistunnels, Zürich, pp 239–252

Lee KM, Rowe RK (1990) Finite Element Modelling of the Three-Dimensional Ground Deformations due to Tunnelling in Soft Cohesive Soils: Part 2—Results. Comput Geotech 10:111–138

Lunardi P (1995) L'importanza del precontenimento del cavo in relazione ai nuovi orientamenti in tema di progetto e costruzione di gallerie. Gallerie e Grandi Opere Sotterranee Marzo (45):16–37

Lunardi P (1998) The influence of the rigidity of the advance core on the safety of the tunnel excavations. Tunnel 8:32–44

Lunardi P (1999) La galleria "Tartaiguille", ovvero l'applicazione dell'approccio ADECO-RS per la realizzazione di un tunnel "impossibile". Gallerie e Grandi Opere Sotterranee 58 (agosto 1999):65–77

Lunardi P (2000) The design and construction of tunnels using the approach based on the analysis of controlled deformation in rocks and soils. In: Tunnels & Tunnelling International special supplement, ADECO-RS approach

Lunardi P (2008) Design and construction of tunnels: analysis of controlled deformation in rocks and soils (ADECO-RS). Springer, Berlin Heidelberg. doi:10.1007/978-3-540-73875-6

Lunardi P, Bindi R (2004) The evolution of reinforcement of the advance core using fibre-glass elements. Felsbau 22(4):8–19

Lunardi P, Focaracci A (1997) Aspetti Progettuali e construttivi della galleria "Vasto". Strade & Construzioni (Agosto 97):72–88

Lunardi P, Focaracci A (1999) The Bologna to Florence high speed railway line: Progress of underground. In: al Ae (ed) Challenges for the 21st Century, Oslo, Norway

Lunardi G, Gatti M (2010) Tunnel monitoring system—a contribution for the preparation of guidelines. In: ITA-AITES World Tunnel Congress 2010—Tunnel Vision Towards 2020, Vancouver, Canada

Lunardi P, Cassani G, Tanzini M (2009) Lo scavo di gallerie di grandi dimensioni nei terreni a grana fine e strutturalmente complessi. Gallerie e Grandi Opere Sotterranee 92 (dicembre):47–60

Madejski J (1960) Theory of non-stationary plasticity explained on the example of thick-walled spherical reservoir loaded with internal pressure. Archiwum Mechaniki Stosowanej 5/6 (12):775–787

Mair RJ (2008) Tunnelling and geotechnics: new horizons. Géotechnique 58(9):695–736. doi:10.1680/geot.2008.58.9.695

Myer LR, Brekke TL, Dare CT, Dill RB, Korbin GE (1981) An Investigation of Stand-up Time of Tunnels in Squeezing Ground. In: Rapid Excavation and Tunnelling Conference, San Francisco, California, pp 1415–1433

Nguyen-Minh D, Corbetta F (1991) New calculation methods for lined tunnels including the effect of the front face. In: 7th Congress of the ISRM, Achen, pp 1334–1338

Oreste P, Peila D, Pelizza S (2004) Face reinforcement in deep tunnels. Felsbau 22(4):20–25

Panet M (1995) Le calcul des tunnels par la méthode convergence-confinement. Presses de l'école nationale des ponts et chaussées, Paris, France

Panet M (2009) Ground behaviour at the tunnel face. In: The evolution of design and construction approaches in the field of underground projects—Rocksoil S.p.A. 30th anniversary conference, Milan

Paulus M (1998) Le tunnel de Tartaiguille. Travaux 742

Peila D (1994) A theoretical study of reinforcement influence on the stability of a tunnel face. Geotech Geol Eng 12:145–168

Pellet FL, Roosefid M, Deleruyelle F (2009) On the 3D numerical modelling of the time-dependent development of the damage zone around underground galleries during and after excavation. Tunn Undergr Space Technol 24(2009):665–674

Perzyna P (1966) Fundamental problems in viscoplasticity. Adv Appl Mech 9:243–377

Ramoni M, Anagnostou G (2010) Tunnel boring machines under squeezing conditions. Tunn Undergr Space Technol 25:139–157

Rossi PP (1995) Il ruolo del monitoraggio negli interventi di miglioramento e rinforzo dei terreni e delle rocce. In: XIX Conegno Nazionale dell'Associazione Geotechnica Italiana, Pavia, Italy

Russo G, Repetto L, Piraud J, Laviguerie R (2009) Back-analysis of the extreme squeezing conditions in the exploratory aid to the Lyon-Turin base tunnel. In: Rock Engineering in Difficult Conditions, Toronto, ON, Canada

Schneider TR (1997) Behandlung der Störzonen beim Projekt des Gotthard Basistunnels. Felsbau 15(6):489–495

Sellner P (2000) Prediction of displacements in tunnelling. Ph.D. thesis, University of Technology, Graz, Austria

Steindorfer A (1998) Short term Prediction of Rock Mass Behaviour in Tunnelling by advanced analysis of displacement monitoring data. In: Riedmüller G, Schubert W, Semprich S (eds) Gruppe Geotechnik Graz, Heft 1. Graz, Austria

Steiner P (2007) Displacement measurements ahead of a tunnel face using the RH Extensometer. In: FMGM 2007: Seventh International Symposium on Field Measurements in Geomechanics

Steiner P, Yeatman R (2009) New instruments improve site characterization with time based measurements. In: Vrkljan (ed) EUROCK 2009—Rock Engineering in Difficult Ground Conditions—Soft Rocks and Karst, Dubrovnik, pp 577–582

Sulem J, Panet M, Guenot A (1987) Closure analysis in deep tunnels. Int J Rock Mech Min Sci 24(3):145–154

Thut A, Nateropp D, Steiner P, Stolz M (2006) Tunnelling in squeezing rock—yielding elements and face control. In: 8th International Conference on Tunnel Construction and Underground Structures, Ljubljana

Trompille V (2003) Etude expérimentale et théorique du comportement d'un tunnel renforcé par boulonnage frontal. PhD Thesis, Ecole National des Travaux Publics de l'Etat, Lyon, France

Vermeer PA, de Borst R (1984) Non-associated plasticity for soils, concrete and rock. Heron 29(3):1–64

Vogelhuber M (2007) Der Einfluss des Porenwasserdrucks auf das mechanische Verhalten kakiritisierter Gesteine. PhD Thesis, ETH Zurich, Zurich, Switzerland

Wong H, Trompille V (2000) Displacement behaviour of a bold-reinforcement tunnel face with finite ground-bolt bond strength: analytical and numerical approaches, in situ data. In: GeoEng 2000, Melbourne

Wong H, Subrin D, Dias D (2000a) Extrusion movements of a tunnel head reinforced by finite length bolts—a closed-form solution using homogenization approach. Int J Numer Anal Methods Geomech 24:533–565

Wong H, Trompille V, Subrin D (2000b) Tunnel face reinforcement by longitudinal bolts: Analytical model and in situ data. In: Miyazaki F (ed) Geotechnical Aspects of Underground Construction in Soft Ground, Kusakabe, pp 457–463

Wong H, Trompille V, Dias D (2004) Extrusion analysis of a bolt-reinforced tunnel face with finite ground-bold bond strength. Can Geotech J 41:326–341. doi:10.1139/T03-084